AGU ADVANCING EARTH AND SPACE SCIENCE

Water Resources Research

RESEARCH ARTICLE
10.1029/2022WR031944

Using Inverse Modeling and Dual Isotopes ($\delta^{15}N$ and $\delta^{18}O$ of NO_3) to Determine Sources of Nitrogen Export From a Complex Land Use Catchment

Sri Adiyanti[1], Yasuyuki Maruya[2], Bradley D. Eyre[3], Perrine Mangion[4], Jeffrey V. Turner[5], and Mathew R. Hipsey[1]

[1]Aquatic Ecodynamics, School of Agriculture and Environment, The University of Western Australia, Crawley, WA, Australia, [2]Graduate School of Engineering, Kyushu University, Fukuoka, Japan, [3]Centre for Coastal Biogeochemistry, Southern Cross University, Lismore, NSW, Australia, [4]UMR ENTROPIE, Université de La Réunion-IRD-CNRS-IFREMER-UNC, La Réunion, France, [5]CSIRO Land and Water, CELS Centre, Perth, WA, Australia

Abstract Attributing nitrogen export to specific land use within heterogeneous catchments remains a challenge due to the spatio-temporal variability in conditions influencing the mobilization and fate of nitrogen species. This study demonstrates that the measurement of dual stable isotopes of nitrate, taken along with routine tributary measurement of nitrogen in nitrate (NO_3^--N) and ammonium (NH_4^+-N), aids in apportioning sources of the overall nitrogen load during wet periods. An inverse modeling technique was developed to estimate the land use-specific export rates of NO_3^--N and NH_4^+-N from the Caboolture River Catchment in Queensland, Australia. Measurements of nitrogen in streamflow at 51 locations during six sampling campaigns (May 2012 to April 2013) were made along with catchment geospatial data that was used to disaggregate sub-catchments into six land use fractions. A hydrological model was applied to compute the runoff from each fraction and water routing through the stream network. This data was used within a nitrogen mixing model with inclusion $\delta^{15}N_{NO3}$ and $\delta^{18}O_{NO3}$. The land uses specific export rate was computed inversely as the posterior of a Bayesian interference applied to the model. During higher rainfall periods when export rates were highest, the main land use exporting nitrogen was wetland (110 g/ha/day NO_3^--N, 27 g/ha/day NH_4^+-N) resulted from mineralization and nitrification of organic N, followed by urban (16 g/ha/day NO_3^--N, 2.3 g/ha/day NH_4^+-N). The advantage of using the dual isotopes in conjunction with the nitrogen concentration data was demonstrated by reduced uncertainty in the computed rates during the higher rainfall periods, relative to calculations without $\delta^{15}N_{NO3}$ and $\delta^{18}O_{NO3}$.

Plain Language Summary Attributing nitrogen export to specific land use types within heterogeneous catchments is difficult. This paper demonstrates the use of an inverse modeling technique, dissolved inorganic nitrogen concentration data, a dual stable isotope measurement data, and geospatial data to estimate the land use-specific export rates of dissolved inorganic nitrogen from six land use types in the Caboolture River Catchment in Queensland, Australia. The results show that during higher rainfall periods when export rates were highest, the main source of nitrogen was found to be wetland (110 g/ha/day NO_3^--N and 27 g/ha/day NH_4^+-N), followed by urban (16 g/ha/day NO_3-N and 2.3 g/ha/day NH_4^+-N).

Key Points:

- An inverse modeling technique was developed to estimate the land use-specific export rate of nitrogen using isotopes signatures
- The model was embedded within a Bayesian framework to assess the predictive uncertainty with and without inclusion of dual isotopes of nitrate
- During wet periods, when nitrogen export rates were highest, the predictive uncertainty was reduced when the model included dual isotopes of nitrate

Supporting Information:

Supporting Information may be found in the online version of this article.

Correspondence to:

S. Adiyanti,
s.adiyanti@gmail.com

Citation:

Adiyanti, S., Maruya, Y., Eyre, B. D., Mangion, P., Turner, J. V., & Hipsey, M. R. (2022). Using inverse modeling and dual isotopes ($\delta^{15}N$ and $\delta^{18}O$ of NO_3) to determine sources of nitrogen export from a complex land use catchment. *Water Resources Research*, *58*, e2022WR031944. https://doi.org/10.1029/2022WR031944

Received 7 JAN 2022
Accepted 16 SEP 2022

Author Contributions:

Conceptualization: Sri Adiyanti
Data curation: Sri Adiyanti, Perrine Mangion
Formal analysis: Sri Adiyanti
Funding acquisition: Bradley D. Eyre
Investigation: Sri Adiyanti, Bradley D. Eyre, Perrine Mangion
Methodology: Sri Adiyanti

1. Introduction

Anthropogenic disturbance of the nitrogen (N) cycle through nitrogen loading from urbanization, industrialization, and agriculture often leads to the eutrophication of downstream receiving water environments (Eyre, 2000; Mayer et al., 2002; Saeck et al., 2013; Smith, 2006; Seitzinger et al., 2010). To understand and manage eutrophication, it is essential to know the sources and sinks of N within a catchment and how they vary in space and time (Eyre et al., 2016). Quantifying the N load from a catchment is routinely performed by multiplying the concentration data from routine river water quality monitoring, C(t), with the river discharge rate Q(t) measured at the catchment outlet. While this estimate is useful for ascertaining the catchment delivery of N to downstream water environments, it is a coarse metric that integrates across the myriad of different N sources and redistribution pathways within a catchment, making it difficult for managers to apportion the overall load amongst specific land use activities. This is particularly the case if the catchment has a complex mosaic of land use and a heterogeneity in landscape properties. This leads to uncertainty as to the dominant anthropogenic driver of N pollution

Project Administration: Bradley D. Eyre, Mathew R. Hipsey
Resources: Bradley D. Eyre
Software: Sri Adiyanti, Yasuyuki Maruya
Supervision: Mathew R. Hipsey
Validation: Sri Adiyanti, Yasuyuki Maruya
Visualization: Sri Adiyanti
Writing – original draft: Sri Adiyanti
Writing – review & editing: Sri Adiyanti, Bradley D. Eyre, Jeffrey V. Turner, Mathew R. Hipsey

and therefore poorly informed management decisions. Furthermore, catchment scale indicators of the extent of denitrification and other processes are essential, for example, whether low N concentrations are due to dilution or denitrification at the catchment scale (Peters et al., 2011; Rassam et al., 2008). As such, there is an ongoing need to develop improved methods to quantify nitrogen export from specific land use types that better informs land management policy and focuses on management interventions to reduce N export.

Developing a comprehensive monitoring network that samples catchment tributaries draining different dominant land uses is a common approach to better delineate hot spots of nutrient export (Seitzinger et al., 2010). However, in many systems, it is rare to be able to find sampling locations that represent a single land use, and in the case of highly heterogeneous catchments all tributaries and river monitoring sites represent a mixing environment of nutrient sourced from various land uses and landscapes. Furthermore, increasing the intensity of anthropogenic impacts on catchments has been reported to increase the functional homogeneity of catchment outputs (Gall et al., 2013), making it difficult to identify which nutrients come from where.

As a result, stable isotopes of nitrogen (N) and oxygen (O) of nitrate (NO_3^-), that is, $\delta^{15}N_{NO3}$ and $\delta^{18}O_{NO3}$, have been gaining increasing use as a means to estimate the dominant land use contributors to stream water quality (Kang et al., 2022; Kendall et al., 2007; Ford et al., 2017; Liu et al., 2021; Rassam et al., 2008). For example, typical $\delta^{15}N_{NO3}$ in manure or sewage of +7‰ to +20‰ (Mayer et al., 2002) is partially distinct from $\delta^{15}N_{NO3}$ in atmospheric deposition (−10‰ to +8‰), $\delta^{15}N_{NO3}$ in synthetic fertilizers (0‰), $\delta^{15}N_{NO3}$ in natural soil (−3‰ to +5‰), and $\delta^{15}N_{NO3}$ produced by nitrification in soil (−20‰ to +10‰) (Kendall et al., 2007). However, due to the overlapping signals, NO_3^- derived from synthetic fertilizers, soils, and the atmosphere typically cannot be distinguished using $\delta^{15}N$ alone. Signatures of $\delta^{18}O_{NO3}$ can inform the process pathways of NO_3^- by identifying the sources of O in NO_3^-, that is, microbial soil nitrification processes ($\delta^{18}O_{NO3}$ <0‰ to +14‰), atmospheric O_2 (ca. +23‰), or environmental H_2O (−30‰ to +5‰) (Kendall, 1998; Kroopnick & Craig, 1972; Mayer et al., 2002). Application of the dual isotopes in NO_3^- ($\delta^{15}N_{NO3}$ and $\delta^{18}O_{NO3}$) has shown potential to support the partial separation of the dominant N sources (atmospheric, mineralization of organic N in forest soils, fertilizers, soil, and sewage) in temperate climate catchments of North America (Mayer et al., 2002), Western Europe (Voss et al., 2006), and Asia (Lee et al., 2008). However, there are no dual isotopes studies in sub-tropical or tropical catchments with heterogeneous land uses, therefore it remains unclear whether the increased information provided for the dual isotopes $\delta^{15}N_{NO3}$ and $\delta^{18}O_{NO3}$ could be of benefit in quantifying the magnitude and variability in land use-specific export rates of nitrogen.

Variability in export rates of nitrogen (with its isotopic signature) occurs not only due to the time-varying nature of human inputs and land management actions, but also due to the highly nonlinear connection between hydrological (mobilization and transport) processes and biogeochemical (transformation) processes (e.g, Eyre & Pont, 2003; Oldham et al., 2013; Turner et al., 2006]. For example, for a given stochastic time-series of rainfall forcing, a disproportionate nutrient load will be released by some events but not others (Gunaratne et al., 2017), due to a decoupling of landscape filtering between hydrological and biogeochemical processes (Gall et al., 2013). However, at the catchment scale, the relationship between flow and export becomes simpler, effective biogeochemical stationarity emerges (Basu et al., 2010). Mechanistic modeling approaches for resolving the dominant pathways of nutrient export from plot to catchment scale have advanced considerably (Paniconi & Putti, 2015). While these approaches are promising in assisting with dis-entangling the time-varying coupling between hydrology and biogeochemical pathways, and provision of land use-specific export rates, they are not always suitable for nutrient export studies since (a) issues around equifinality create considerable uncertainty as to whether they can accurately resolve the pathways based on limited calibration data (Houska et al., 2017), and (b) the mechanistic modeling approach requires numerous inputs of nutrients to the landscape (e.g., fertilizers) to be provided as boundary conditions, which is a challenge for catchment managers since this data can be difficult to source, or unreliable.

The aim of this study was to estimate land use-specific export rates of dissolved inorganic nitrogen by developing an inverse approach that hybridizes results from a distributed hydrological model (DHM) with empirical geospatial and river nutrient monitoring data. The inverse calculation adopts a Bayesian Hierarchical Framework using a Markov-chain Monte Carlo (MCMC) state-space algorithm to address the challenge that the measured isotope signatures do not represent unequivocal end-member signatures due to the samples being collected in isotopically mixed environments. The approach was applied with and without the inclusion of isotope data to demonstrate that stable isotope measurements taken along-side routine stream nutrient sampling can improve

the accuracy of source apportionment of the overall nitrogen load. The results demonstrate the relative benefit of including isotope data as an information constraint on the nutrient export calculation in both wet and dry flows, and improvements to extend the approach are outlined.

The proposed work is not directed toward further development and understanding of biogeochemical cycling of N, but the conceptual advance made here is to demonstrate that it is possible to identify and quantify N contributions to streamflow from a multiple land use catchment. Furthermore, the analysis is based at the scale of land use units, which is the scale at which catchment managers normally require information and are able to enact management decisions to minimize N export via discharge.

2. Approach and Methods

The approach was applied to the Caboolture River catchment in southeast Queensland, Australia. A distributed river discharge 1K-Distributed Hydrological Model (1K-DHM) (Sayama & McDonnell, 2009; Tanaka & Tachikawa, 2015) was utilized that takes into account saturated through-flow processes to predict land use-specific runoff rates. The land use-dependent hydrological parameters in 1K-DHM were optimized using the shuffled complex evolution (SCE) method (Duan et al., 1993, 1994). The 1K-DHM output discharges were then used as input to an isotope mixing model within a Bayesian Hierarchical Framework to inversely simulate the land use-specific dissolved inorganic nitrogen exports. The model outputs are the posteriors of the dissolved nitrogen export rate (mg/ha/day) for each of the land use types. This was done for six individual sampling between May 2012 and April 2013 that captured the dry and wet seasonality of water quality, as recorded at 51 sampling sites within the catchment domain.

2.1. Study Site

The Caboolture River Catchment is a sub-tropical catchment in southeast Queensland, Australia, approximately 40 km north of Brisbane (Figure 1). It has a catchment area of 383 km^2 with elevations ranging from 0 to 550 m above sea level. The complex stream network is an amalgamation of Wararba Creek, Lagoon Creek, King Johns Creek, Gregor's Creek, Sheepstation Creek, and Gympie Creek, which discharge to the main Caboolture River and downstream Caboolture Estuary Mouth, with final discharge to Deception Bay, a small embayment within the larger Moreton Bay (Figure 1).

Rainfall data measured at 10 Bureau of Meteorology (BoM) stations and temperature data at the BoM Beerburrum Meteorological Station, 20 km north-west of Caboolture (Figure 1) was utilized. Gridded rainfall was calculated using an inverse distance weighting method that captured the spatial variation of rainfall within the area, which was higher in the mountain areas compared to the lowland areas. The long-term (1910–2015) average of annual rainfall measured at Beerburrum Station was 1,253 mm. On average, the highest monthly rainfall occurs in February (204 mm) during the late summer-autumn wet season and the lowest during the mainly dry winter in July (32 mm), reflecting typical sub-tropical seasonal variations.

The major land uses in the Caboolture River Catchment include crops (11%), conservation and forests (22%), livestock (16%), rural (35%), urban (9%), river and creeks (6%), and wetland (1%). In the upper catchment, the dominant land uses are forest, crops, and livestock. Crops are largely dominated by fruit trees and pineapples and to a lesser extent, berries. Orchards and mango plantations are mostly in the upper Wararba Creek and Caboolture River sub-catchments, while pineapples and berry plantations are mainly present in the upper Lagoon Creek sub-catchment. The middle catchment is characterized by rural and urban usages such as residential and commercial/industrial. In the lower catchment, wetland and rural are the dominant land uses (Figure 1). Scattered livestock farming is present at the lower catchment with mainly beef and dairy cattle grazing on large areas of native pastures located near water courses.

2.2. Measurement, Water Quality Sampling, and Analysis

Water quality samples were collected at 51 field sites during six sampling campaigns within the Caboolture River (CR) catchment above the tidal limit (Figure 1) as follows: CR_5 (May 29–30, 2012), CR_7 (August 15–16, 2012), CR_9 (October 9–11, 2012), CR_{11} (December 11–13, 2012), CR_{13} (February 4–8, 2013), and CR_{15} (April 24–25, 2013). CR_7 and CR_{15} represent dry season and CR_5, CR_9, CR_{11}, and CR_{13} represent wet season. The water quality

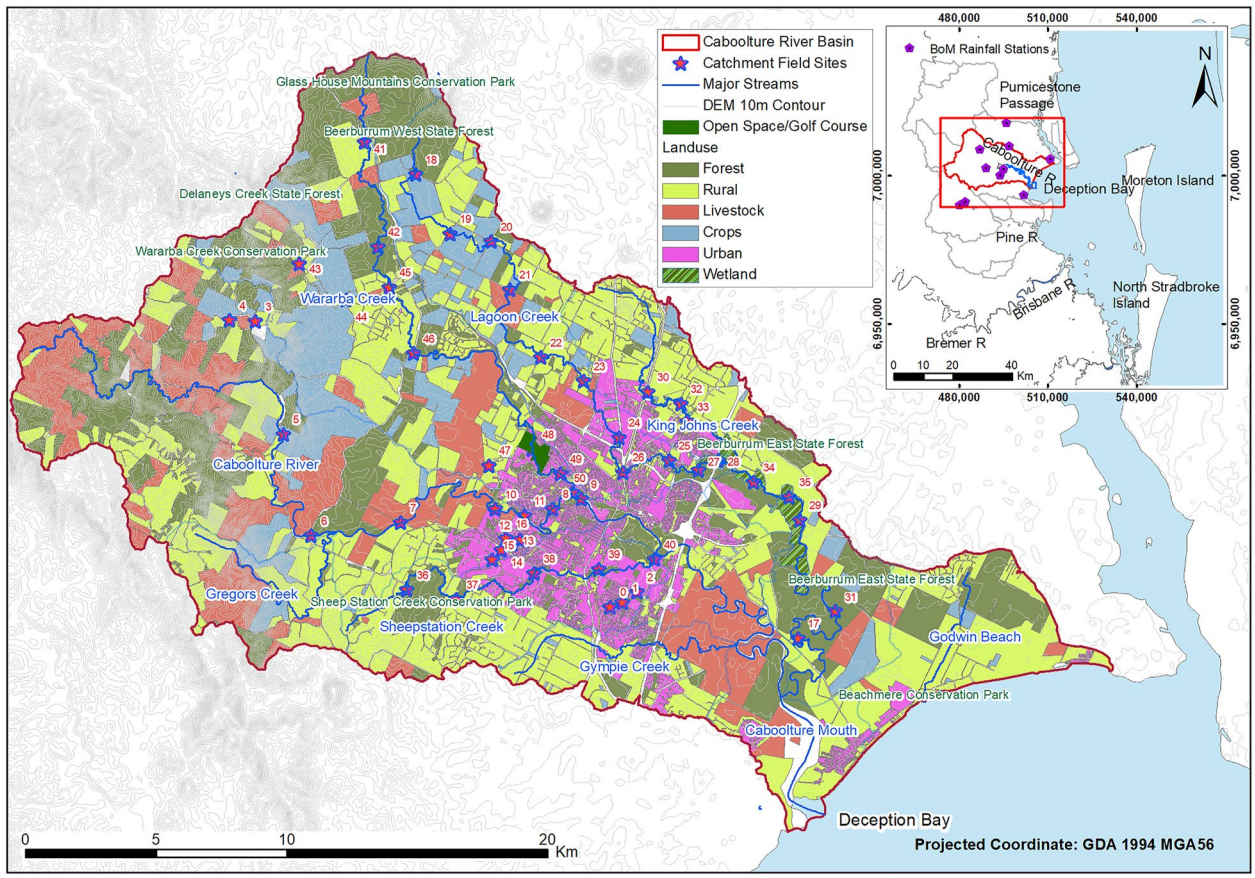

Figure 1. Caboolture River catchment field sites (identification numbers 0–50) and land use types, with 10 rainfall stations provided in the inset.

parameters include concentrations of dissolved inorganic nitrogen as nitrate NO_3^--N and ammonium NH_4^+-N and dual isotopes of NO_3^- ($\delta^{15}N_{NO3}$ and $\delta^{18}O_{NO3}$).

At each location, surface water was collected with a water sampling pole holding a sample-rinsed polypropylene container. Samples for ammonium (NH_4^+), oxides of nitrogen (NO_x^-), and stable isotopes of NO_3^- ($\delta^{15}N_{NO3}$ and $\delta^{18}O_{NO3}$) analyses were immediately filtered through sample-rinsed cellulose acetate membrane filters with a 0.45 and 0.2 µm pore size, respectively. All water samples were stored in polypropylene vials, kept cold on ice, and frozen at the end of the sampling day.

The concentrations of NO_3^- and NH_4^+ were determined colorimetrically using LachatTM flow-injection analysis (McKee et al., 2000). Analytical accuracy for nitrogen analysis was maintained using standard additions of certified laboratory standards in Milli-Q water. The isotopic composition of nitrate ($\delta^{15}N_{NO3}$) was determined using the denitrifier method (Casciotti et al., 2002; Sigman et al., 2001). This method results in the complete conversion of NO_x^- into N_2O by the specific strain of bacteria *Pseudomonas aureofasciens* (ATTC #13985). The produced N_2O was subsequently concentrated and purified in a custom-built purge and trap system. Analysis of its isotopic composition was performed using a Delta V Plus IRMS (Thermo Fisher Scientific) with a modified Gas Bench II interface (Erler et al., 2015). Data were subsequently normalized using certified reference materials. USGS 32 and USGS 34 were used for calibrating $\delta^{15}N$ values with respect to atmospheric N_2, while USGS 34 and USGS 35 were used to express $\delta^{18}O$ values relative to the reference VSMOW scale (Böhlke & Coplen, 1995; Böhlke et al., 2003).

All $\delta^{15}N$ and $\delta^{18}O$ results are expressed as per mille (‰) with reference to the international standard as:

$$\delta^{15}N\,(‰) = \left[\left(15N/^{14}N_{Sample}\right) / \left(15N/^{14}N_{standard}\right) - 1\right] \times 1000 \quad (1a)$$

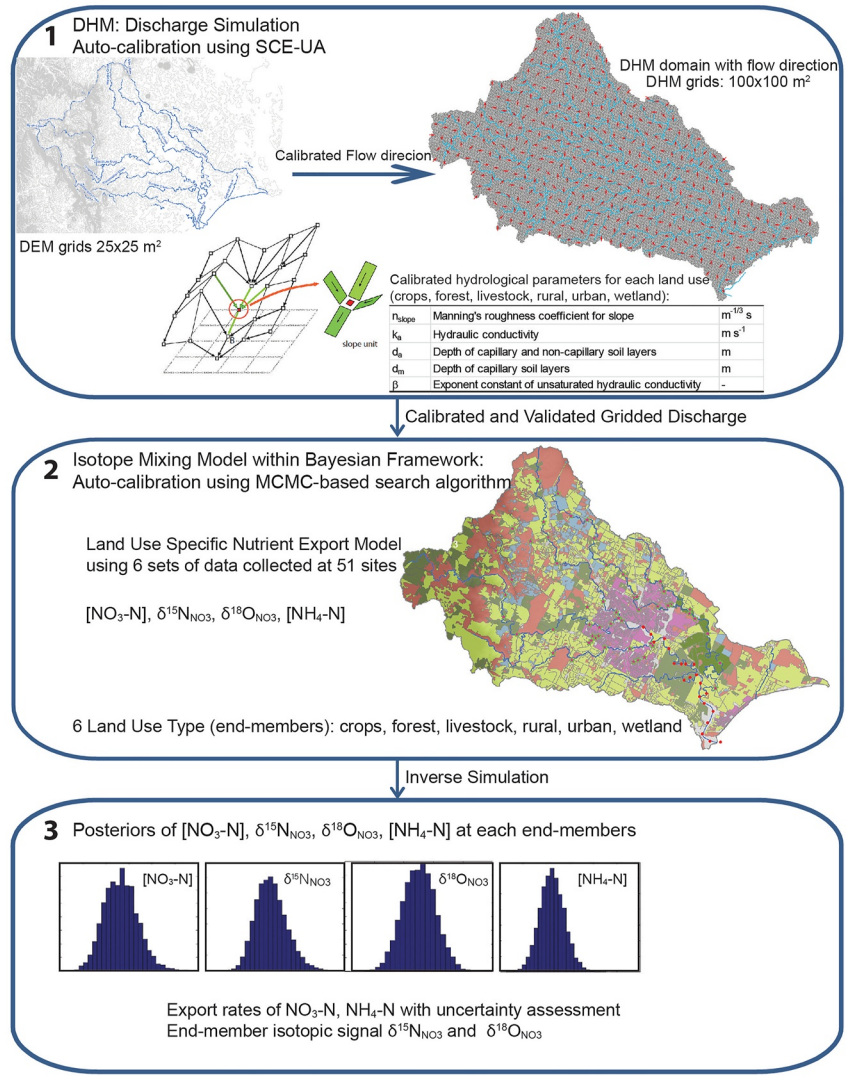

Figure 2. Model framework.

$$\delta^{18}O\,(‰) = \left[\left(18O/^{16}O_{Sample}\right) / \left(18O/^{16}O_{standard}\right) - 1\right] \text{ x } 1000 \quad (1b)$$

where $^{15}N/^{14}N_{standard}$ is 0.0036765 (AIR) and $^{18}O/^{16}O_{standard}$ is 0.0020672 (VPDB).

In addition, the reference material IAEA NO_3 was used as a quality control and run in triplicates in each batch of analysis to ensure good accuracy. The precision of the method depends on sample NO_3^--N concentrations. For samples with NO_3^--N concentrations greater than 1 µmol/L, the within-lab reproducibility as estimated by the pooled standard deviation was 0.2‰ and 0.3‰ for $\delta^{15}N_{NO3}$ and $\delta^{18}O_{NO3}$, respectively. For samples having NO_3^--N concentrations between 0.2 and 1 µmol/L, the within-lab reproducibility was 0.5‰ and 0.8‰ for $\delta^{15}N_{NO3}$ and $\delta^{18}O_{NO3}$, respectively. Results from samples with NO_3^- concentrations lower than 0.2 µmol/L were not included in the study as the analytical error was too large. Isotope δ values were reduced from relative abundances to the state variable mass used in numerical processing.

2.3. Model Framework

The model framework adopts a three-step process (Figure 2). First, the model watershed containing flow direction and accumulation was constructed using a GIS watershed tool on a 25 × 25 m^2 grid digital elevation model

(DEM) and calibrated using the reference stream network provided by the Queensland Government. The calibrated watershed was applied to the distributed hydrological model 1K-DHM (Tanaka et al., 2015) to compute the gridded discharge $Q(x,y)$. The DHM was then calibrated by comparing the simulated discharge against the daily discharge observed at the Upper Caboolture gauging station (142001A) for five periods: (a) January 1–31, 2011 (representing the 1-in-100 years Average Recurrence Interval (ARI) flood event on January 11, 2011), (b) January 1–31, 2012 (wet summer condition), (c) May 1–31, 2009 (wet autumn), (d) May 1–31, 2012 (dry autumn), and (e) multiple months from January 1 to March 31, 2012. Second, the simulated discharge $Q(x,y)$ was incorporated into an isotope mixing model within a Bayesian Hierarchical Framework that inversely simulated the six land use (end-member) concentrations of NO_3^--N and NH_4^+-N and stable isotopes $\delta^{15}N_{NO3}$ and $\delta^{18}O_{NO3}$. The model was auto-calibrated against the NO_x^--N and NH_4^+-N concentrations and stable isotope signatures measured at the 51 sampling sites (Figure 1) during the six sampling campaigns (CR_5, CR_7, CR_9, CR_{11}, CR_{13}, and CR_{15}) between May 2012 and April 2013. Third, the inversely simulated posteriors of nitrogen concentrations for each land use were then converted into the land use-specific nutrient export rate of NO_3^--N and NH_4^+-N. Each posterior contains information of the central tendency (i.e., mean and median) and variability (i.e., standard deviation) of each possible population of the export rate, providing model uncertainty information.

2.3.1. Distributed Hydrological Model 1K-DHM and Calibrations

The 1K-DHM is a DHM based on a kinematic wave flow approximation that takes into account surface and subsurface flows using a storage-discharge equation. The kinematic flow was applied to each grid within the DHM, where flow was defined as a net of rainfall input and evapotranspiration loss into the grids and discharge from upstream cells (Tanaka & Tachikawa, 2015),

$$\frac{\partial A}{\partial t} + \frac{\partial Q}{\partial x} = r - e \tag{2}$$

$$Q = \sqrt{I}/n_c\, B^{-3/2} A^{3/5} \tag{3}$$

where A is the cross-sectional area, Q is the discharge, t is time, x is distance, r is rainfall intensity, e is evapotranspiration, I is the slope gradient, n_c is Manning's roughness coefficient, and B is the width of river channel. The values for rainfall at each grid were calculated using an inverse distance weighting method, and values for evapotranspiration were estimated using an empirical relationship between monthly air temperature and evapotranspiration measured at Beerburrum Station. Details are provided in Figure S3 in Supporting Information S1.

The flow direction in the dendritic stream network of the Caboolture River catchment was derived from 25×25 m^2 grid DEM of the basin using a GIS watershed tool, which was validated against the reference stream network. The comparison between the derived and reference stream networks is provided in supporting material S1. The land use type for each grid was identified by overlaying the model grids with the surveyed land use map. The dominant land use was assigned for the grid with multiple land use identified (Figure 2).

Based on the number of upslope cells, each cell was assigned as either a river-channel cell or a slope-runoff cell. Flow from a river-channel cell was modeled using Equations 2 and 3, whereas flow from a slope-runoff cell was modeled using modified equations that take into account both saturated and unsaturated subsurface flow components (Hunukumbura et al., 2012; Sayama & McDonnell, 2009),

$$\frac{\partial h}{\partial t} + \frac{\partial q}{\partial x} = r - e \tag{4}$$

$$q = \begin{cases} d_c k_c \left(\dfrac{h}{d_c}\right)^{\beta} i, & \text{for } 0 \le h \le d_c \\ d_c k_c i + (h - d_a)\, k_a i, & \text{for } d_c \le h \le d_a \\ d_c k_c i + \dfrac{\sqrt{i}}{n_s}(h - d_a)^m + (h - d_a)\, k_a i, & \text{for } d_a \le h \end{cases} \tag{5}$$

where h is the water stage, q is the discharge per unit slope width, d_c is the water stage equivalent to the maximum water content in capillary pores, i is the slope, d_a is the water stage equivalent to maximum water content in

effective porosity, n_s is Manning's surface roughness coefficient for overland flow, k_c is the hydraulic conductivity when capillary pores saturated, and k_a is the saturated hydraulic conductivity calculated as,

$$k_a = \beta k_c \tag{6}$$

where β is an exponent parameter of the q-h relationship shown in Equation 5. Parameters n_s, k_a, d_a, d_c, and β of each land use (except urban) were optimized. As for urban, only parameter n_s was optimized as urban surface water runoff is controlled via drainage and stormwater system, hence d_a is negligible, $d_c = 0$, and $\beta = 1$.

The DHM setup requires 30 sets of parameters (i.e., 5 parameters n_s, k_a, d_a, d_m and β for the 6 land use types) to calibrate, for which the Shuffled Complex Evolution of University of Arizona (SCE-UA) was applied due to its robustness and efficiency as a global optimization method for calibration of rainfall-runoff models (Duan et al., 1993, 1994). The algorithm combines the best features of multiple complex shuffling and competitive evolution which enable a parallel exploration of the search space by using a population of potential solutions.

The SCE-UA steps in this study include the generation of initial population sampled randomly from a search space ($n = 1{,}000$) and the partition of the population into two complexes, each containing 51 points. Within each complex, the population reproduces and evolves based on simple geometric shapes and Nash-Sutcliffe efficiency (NSE; Nash & Sutcliffe, 1970), directing the search toward a global convergence within 6–7 generations.

The DHM simulations were first run for calibration against daily discharge measured during the five calibration periods (Section 2.3). Inputs to the model included daily gridded rainfall, temperature and evaporation loss, and initial DHM parameters for each land use. The calibration resulted in five sets of n_s, k_a, d_a, d_m, and β for each land use, from which the average of parameter values over the five periods were calculated for each land use and applied to the DHM simulation during May 1, 2012 to April 1, 2013. The output of the DHM daily simulation (gridded discharges) was applied in the isotope mixing—nutrient export model. At this point, each grid (of 100×100 m^2) contained information on discharge and land use type.

2.3.2. Stable Isotope Mixing Model—Nutrient Export Model

Stable isotope mixing models are often used to estimate the source contributions to a mixture. However, the number of sources that can be partitioned is limited by the number of isotopic signatures employed. Application of dual ($n = 2$) isotope $\delta^{15}N_{NO3}$ and $\delta^{18}O_{NO3}$ is capable of estimating up to three sources ($n + 1$) contribution of NO_3^-. To estimate the contribution from many sources, a priori and a posteriori aggregation methods (Phillips et al., 2005) were used.

Our model utilizes an a priori and a posteriori aggregation approach based on a Bayesian Framework that uses an MCMC algorithm (Adiyanti et al., 2016). The model estimates the posteriors of land use-specific contributions of NO_3^--N, NH_4^+-N and dual isotopes signatures of NO_3^- using an inverse technique applied to the nutrient mixing model. This was done by optimizing the modeled concentrations (mg/L) and isotope data (‰) against the values measured at each station i ($i = 1, \ldots, 51$), shown in Equations 7a–7e,

$$\delta^{15}N_i = \sum_{j=1}^{6} \left(f_{i,j}.\delta^{15}N_{j,post}\right) \tag{7a}$$

$$\delta^{18}O_i = \sum_{j=1}^{6} \left(f_{i,j}.\delta^{18}N_{j,post}\right) \tag{7b}$$

$$NO_3^-N_i = \sum_{j=1}^{6} \left(f_{i,j}.NO_3^-N_{j,post}\right) \tag{7c}$$

$$NH_4^+N_i = \sum_{j=1}^{6} \left(f_{i,j}NH_4^+N_{j,post}\right) \tag{7d}$$

where $\delta^{15}N_i$, $\delta^{18}O_i$, $NO_3^-N_i$, and $NH_4^+N_i$ are the simulated isotope signatures $\delta^{15}N_{NO3}$ and $\delta^{18}O_{NO3}$, concentrations of NO_3^--N and NH_4^+-N at each station i; and $f_{i,j}$ is the fraction of discharge from each land use at each station.

The $\delta^{18}O_i$ values were approximated as a function of $\delta^{15}N_i$, therefore Equation 7b can be reformulated as,

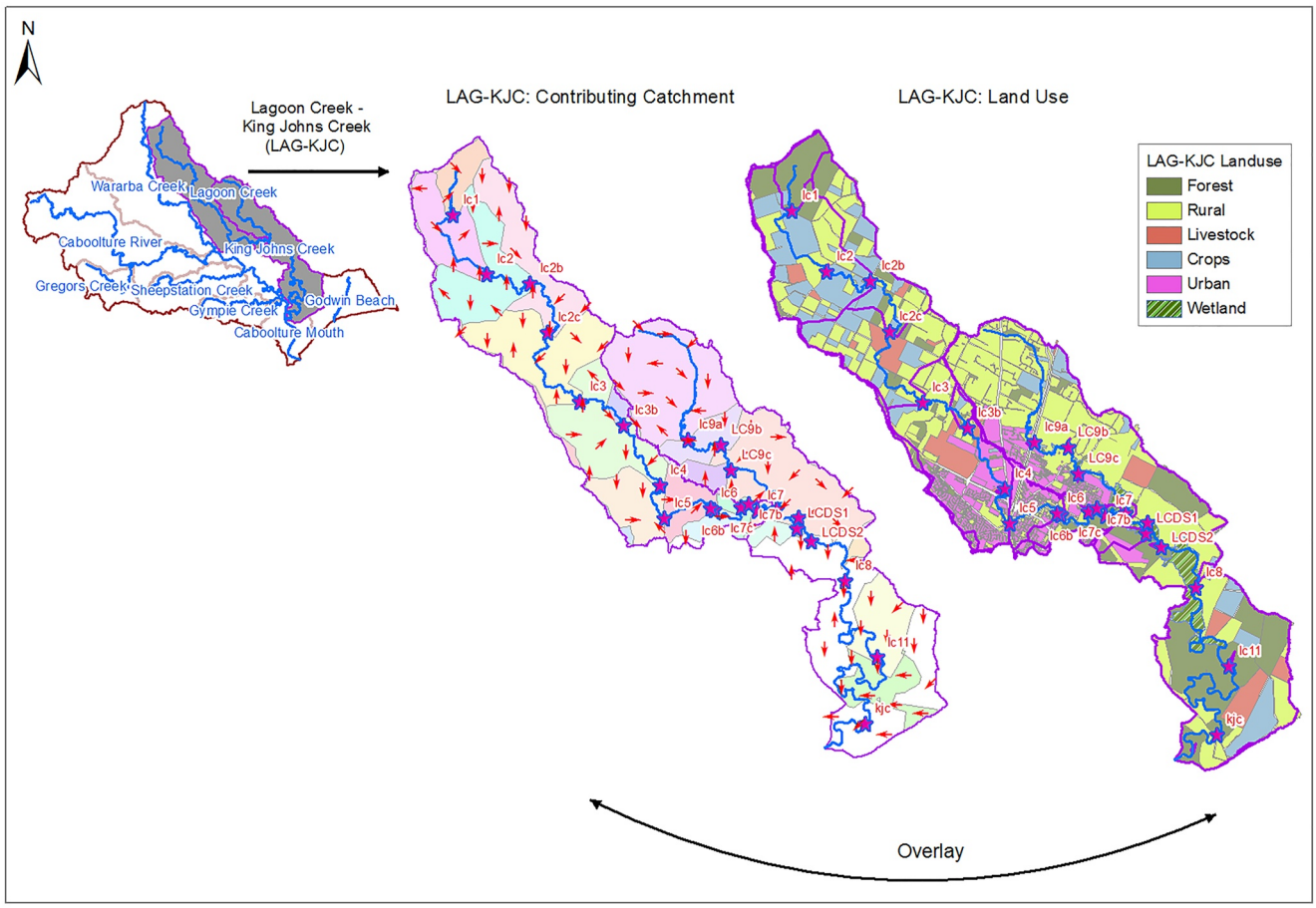

Figure 3. Sub-watershed delineation and land use.

$$\delta^{18}O_i = \sum_{j=1}^{6} \left(f_{i,j} . \left(m_j . \delta^{15}N_{j,post} \right) \right) \tag{7e}$$

where m_j is the gradient in the $\delta^{15}N$ and $\delta^{18}O$ relationship for each land use j. The gradient values of the derived linear regression of measured signals of $\delta^{15}N_{NO3}$ and $\delta^{18}O_{NO3}$ (details in Section 4.1) were used as priors.

The fraction of discharge from each land use (j) at each station (i), $f_{i,j}$, where j represents crops, forest, livestock, rural, urban, and wetland) was calculated as,

$$f_{i,j} = \frac{A_{i,j}}{A_i} Q_i \tag{8}$$

where $A_{i,j}$ is the sub-watershed area for each land use j at each station i which was determined from the contributing grids to each of the 51 stations (A_i) using a GIS watershed delineation tool which was further overlain with the surveyed land use map (Figure 3), and Q_i is the DHM simulated discharges at each station i (Section 2.3.1).

The contributing catchment grids to each station i were developed using a GIS watershed tool applied on the flow direction and accumulation grids derived from the DHM simulation (Step 1). Each grid (of 100 × 100 m^2) containing information of discharge and land use proportions was identified as a contributing grid to one of the 51 stations, enabling the calculation of $f_{i,j}$.

The solutions to Equations 7a–7e are a set of posteriors of land use-specific $\delta^{15}N$ and $\delta^{18}O$ signatures and concentrations of NO_3^--N and NH_4^+-N, depicted as $\delta^{15}N_{j,post}$, $\delta^{18}O_{j,post}$, $NO_3^-N_{j,post}$, $NH_4^+N_{j,post}$ in Equations 7a–7d.

The right side of Equations 7c and 7d resulted in concentration posteriors at each of the six land uses ($NO_3^-N_{j,post}$, $NH_4^+N_{j,post}$) which were then converted into the land use specific export rates (mg/ha/day) of NO_x^--N and NH_4^+-N using:

$$NO_3^- N_{export} = NO_3^- N_{j,post} . \frac{Q_j}{A_j} \tag{9a}$$

$$NH_4^+ N_{export} = NH_4^+ N_{j,post} . \frac{Q_j}{A_j} \tag{9b}$$

where Q_j and A_j are the total discharge and area of each land use in the model domain.

2.3.3. Bayesian Interference and Adaptive Markov-Chain Monte Carlo

The procedures for calibrating conceptual models have progressed rapidly in the last decade as a result of advances in computing simulations that have the ability to reduce the computational demands of iterative processes. The progress has enabled the calibration of multi-dimensional parameters to be performed effectively to satisfy the necessary criteria, that is, ability to avoid being trapped in the local maxima and minima during the search in the objective function evaluation, and robustness in the presence of different levels of parameter sensitivity and interdependence. This in turn results in a global convergence in the presence of multiple regions of attraction within the search area. An example of such a procedure is Bayesian inference—MCMC (Zhang & Arhonditsis, 2009), which was used in this study.

The central aim in applying an MCMC framework for calibration is to reduce the ambiguity that otherwise appears when one uses a single set of parameters for calibration as part of a manual calibration (Adiyanti et al., 2016), which is based on Arhonditsis et al. (2008). Bayesian interference considers that measurements (Y), sometimes termed as a data model from a Bayesian perspective, and the unknown process model (X) and model parameters (θ) contain uncertainties. These can be estimated by simultaneously calculating the conditional probability of data model Y given the process model X and model parameters θ, i.e., $p\left(\left[Y_{T_1}\ldots,Y_{T_n}|X_1,\ldots,X_T,\theta\right)\right.$ or shortened as $p(Y|X,\theta)$, the conditional probability of the process model given the parameter $p(X_1,\ldots,X_T|\theta)$ or $p(X|\theta)$ using the prior information of the parameter values $p(\theta)$. This allows calculation of the probability of the parameter posteriors, or joint probability of the process model and model parameters given the data model $p(X,\theta|Y)$. The unknown probability of the process model $p(X)$ can be estimated through sampling the posteriors $p(X|\theta)$ and joint probability $p(Y,X,\theta)$ in the MCMC framework.

The Bayesian-MCMC is a specialization of the general Bayesian Hierarchical Model that imposes the Markov property on the state process $\psi(t)$, that is, the current state depends only on the most recent previous state in the Markov-chain. The framework simultaneously calculates the probability of model parameters given the process model or posteriors $p(\theta|\psi)$ and the probability of the data model given the parameters at the state $p(Y|\psi,\theta)$ to produce a better representation of the joint distribution for prediction. In our study, the state is evaluated as the sum of the square of errors (SSE) between the model and observed concentrations at all 51 stations during the six sampling campaigns (CR). Due to outliers observed with NO_3^--N and NH_4^+-N concentrations, the data was bound to the 95% percentile.

The Metropolis-Hastings MCMC algorithm was applied to draw samples from the Bayesian distribution as summarized in the following five steps (Adiyanti et al., 2016; Harmon & Challenor, 1997): (a) a starting vector $\varphi_{t=0}$ was drawn from a prior distribution $p(\varphi)$ for the Markov-chain, where vector φ consists of 24 model parameters (i.e., 4 source concentrations for each 6 land use with the same priors values for each land use) and 4 initial conditions that were optimized, (b) a new vector φ' was generated from a distribution $q(\varphi',\varphi)$and a random number u from a uniform distribution $U(0,1)$, (c) the probability of the move in the Markov-chain $\alpha(\varphi,\varphi') = \pi(\varphi')\,q(\varphi',\varphi)\,/\pi(\varphi)q(\varphi,\varphi')$ was computed where π is the target distribution, (d) if $u \le \alpha(\varphi,\varphi')$ then φ' was accepted as the next state φ_t in the chain, otherwise φ was kept as the next step in the chain, and (e) steps 2–4 (random walk Metropolis) were repeated and evaluated until the Markov chain became time-reversible and had stationary probabilities $\pi(i)P_{i,j} = \pi(j)P_{j,i}$ for $j \ne i$. The adaptive Metropolis and delayed rejection (Haario et al., 2006) were applied to improve the convergence of the solution.

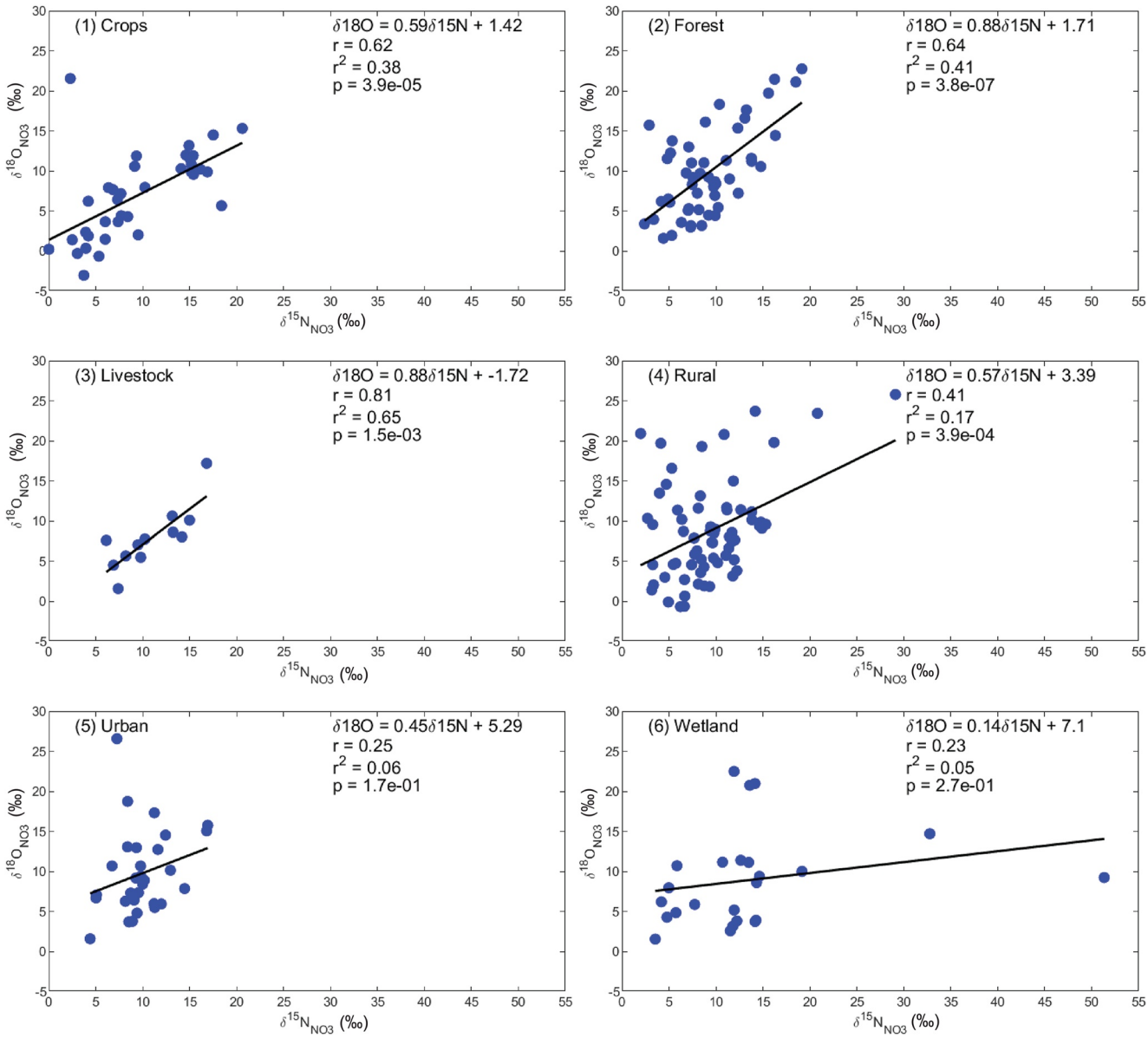

Figure 4. Scatter plots of dual isotopes $\delta^{15}N_{NO3}$ (‰) and $\delta^{18}O_{NO3}$ (‰) sampled in mixing environment from six land uses. Land use was identified based on the predominant land use immediately upstream the creek or streamflow where the samples were taken from. The gradients in the linear regression of $\delta^{18}O_{NO3} = f(\delta^{15}N_{NO3})$ were applied as priors of parameter m_j in Equation 7e.

The following Bayesian-MCMC routine was executed for the dry and wet periods separately, with each containing two and four sampling campaigns, respectively. Observed values for each land use (Figure 4) were applied as an initial set of parameters (priors) for both periods. The initial chains were first run for 6,000 iterations and the results were used to initiate the next 5,000 iterations. About 70%–75% of the proposed solutions were accepted, from which the posteriors were sampled. Three chains were run separately, and their running averages and variances were monitored. Algorithm stability was indicated when all the three chains converged to similar solutions. Output of the routine includes 24 posteriors of land use-specific (end-member) parameters (isotope signatures and nitrogen concentrations) and 4 posteriors of initial values, which were then converted into land use-specific export rates of NO_3^--N and NH_4^+-N, and the corresponding $\delta^{15}N_{NO3}$ and $\delta^{18}O_{NO3}$.

To ensure that the necessary condition for convergence of the solutions was satisfied, three diagnostics were assessed at the end of MCMC routine execution: (a) convergence evolution visually using SSE plots for all

the chains, (b) convergence solution statistically using the Geweke's spectral density diagnostic (Brooks & Roberts, 1998; Geweke, 1992), and (c) the posterior distribution plots. The second diagnostic is based on the test for equality of mean estimates of the first 10% and the last 50% of chains using the power spectral density Hanning window. If the samples are drawn from the stationary distribution of the chain, the two means are equal and the Geweke's statistic has an asymptotically standard normal distribution. By using the above three diagnostics, the problem identified in implementing MCMC simulation caused by the transient phase of the Markov chain to reach the stationary phase (Brooks & Roberts, 1998) can be avoided.

To illustrate the model uncertainty due to model parameters and data model (observations) $[X|Y,\theta]$, the Bayesian model predictions were calculated using the Generalized Gaussian Error Technique (Grabe, 2010), $y_i = \mu + \varepsilon_i$; where ε_i denotes random errors calculated from random number multiplied the standard deviation of all simulated state variable values at all sites. This was done by running the mixing model using 1,000 random samples drawn from the 28 posteriors output from the MCMC routine each for dry and wet periods, hereinafter referred to as the Bayesian mixing model.

2.3.4. Models Performance Assessment

The performance of DHM was assessed using validation metrics—residual and correlation methods that is, NSE, Root Mean Square Error (RMSE), Normalized RMSE (RSR), and Bias (Bennett et al., 2013; Moriasi et al., 2007; Nash & Sutcliffe, 1970) and time-series plots.

To illustrate the role of isotope signatures in the performance of land use specific nitrogen export model, the N (of NO_3^- and NH_4^+) export model was run without the inclusion of isotopes $\delta^{15}N_{NO3}$ and $\delta^{18}O_{NO3}$ using the same routine as for the isotope-enabled model. Both models' results were compared using the same validation metrics (NSE, RMSE, RSR, Bias, r, and r^2).

3. Results

3.1. Isotope Signatures in the Mixing Environment

The scatter plot of observed $\delta^{15}N_{NO3}$ and $\delta^{18}O_{NO3}$ (Figure 4) indicates the significant linear relationship ($p << 0.01$) between the signatures measured in mixing environments with the majority land use identified as crops, forest, livestock, and rural. A strong correlation ($r > 0.6$) exists for crops, forests, and livestock, that is, about 38%, 41%, and 65% variation in $\delta^{18}O_{NO3}$ signatures can be predicted from the linear relationship with $\delta^{15}N_{NO3}$, and a weak correlation ($r < 0.5$) for rural. There is no significant correlation between the dual isotopes signatures for urban and wetland land uses, which may be due to the fact that urban receives more variable sources and wetland experiences more biogeochemical processing, including formation of organic nitrogen and nitrification (indicated with a high range of $\delta^{18}O_{NO3}$) than other land uses.

3.2. Distributed Hydrological Model Discharge Calibration

The DHM simulated the daily discharges fairly well over an order of the magnitude 10^{-1} to 10^2 m^3/s (Figure 5). All calibrations produced NSE of greater than 0.5, but residuals (RMSE, RSR, and Bias) varied depending upon the magnitude of the peak discharges. Among the five calibration periods, the May 2012 calibration (Figure 5d) indicates the best fit with a high NSE, and small RMSE, RSR, and Bias. The good calibration reflects the significant difference between the peaks of small discharges (10^{-1} m^3/s). Detailed calibrated parameters values are provided in the Supporting Information S1.

A fair agreement was achieved between the DHM-modeled daily discharge and the measurements (Figure 5) suggesting that the DHM was able to reproduce seasonal hydrological variations. The inaccuracy in reproducing the peak magnitude suggests the daily resolution applied in the simulation might not capture the diurnal variation in discharges. Note that DHM was primarily developed to estimate floods, and as such it does not have the capability to take into account the time-variant storage capacity, as such all the five calibrated parameters were assumed constant throughout the simulation. This resulted in overestimated discharges in November–December 2012 and April 2013 (Figure 5f) with an overall bias of 2.4 m^3/s. Nevertheless, for the purpose of the study

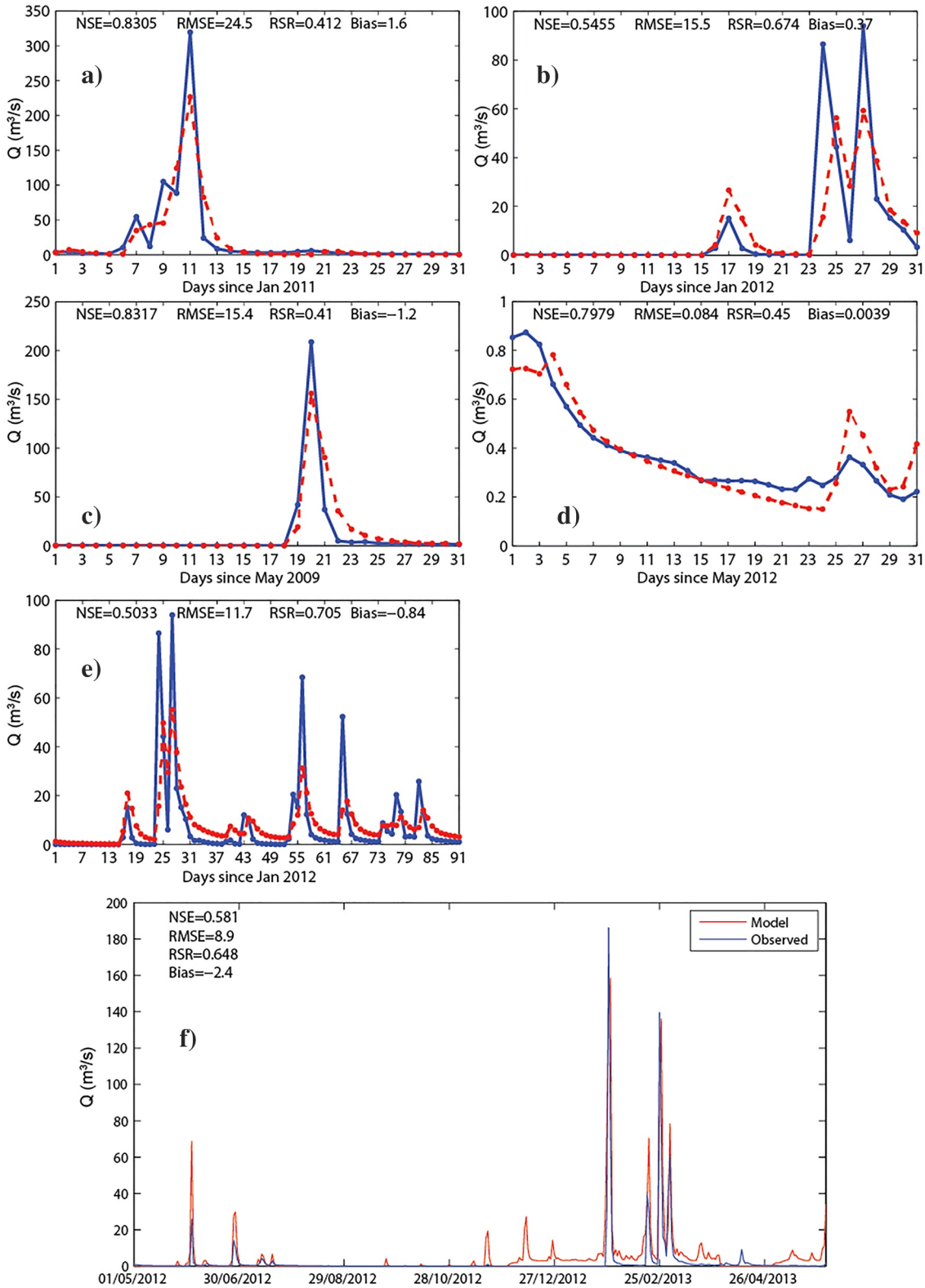

Figure 5. DHM Discharge Calibration (a–e) and Validation (f), with NSE, RMSE, RSR (=RMSE/Standard deviation of observation), and Bias are provided.

where the nutrient data was only available at a lower resolution (bimonthly) than the hydrological forcing, it was concluded that a daily resolution of DHM was adequate.

3.3. Nitrogen Export Model Posteriors and Bayesian Mixing Model

Figure 6 illustrates the resulting posteriors distribution for forest land use, that is, $\delta^{15}N_{j,post}$, $\delta^{15}N_{j,post}$, $NO_3^-N_{j,post}$, and $NH_4^+N_{j,post}$ depicted in Equations 7a–7d. The prerequisite for MCMC calibration to have sufficiently low-dependence between parameters during randomization is satisfied, as indicated by small Pearson's correlations (r) and small covariance values (Cov) shown in the upper right triangle of panels in Figure 6. As a result, their standard errors are representative of uncertainty in the estimate. Table 1 details the posteriors of the 24 parameters for dry and wet periods for each land use.

The number of optimized parameters (24 model parameters and 4 initial conditions) relative to the number of observed values (i.e., 4 state variables at 51 sites; 2 sets of samples in the dry and 4 in the wet season) limits the capability to reduce the model uncertainty due to a high range of values in the observed data. It was also found that the number of parameters being optimized (28 parameters altogether) reached the maximum number of parameter that MCMC can handle. This was indicated by the mean of posterior values changing slightly with new simulation runs, although the region of solutions (distribution with 95% confidence interval) were still within the expected distribution as shown in the Gaussian plots of parameter covariance matrix (examples in Figure 6 and Figures S4 and S5 in Supporting Information S1).

The simulated discharges in the dry period (August 2012 and April 2013; Figure 5f) were all small (<0.01 m^3/s in average) and the observed nitrate and ammonium concentration were elevated (Figure 7a). For this case, the mixing model was not sensitive in capturing the land use effect on nitrogen exports. This was reflected as high uncertainty in the process model due to parameter posteriors $p(\psi|\theta)$, shown in dark gray band in Figure 7a. The 1K-DHM simulates surface (high) flow and subsurface (low) flow or baseflow. Groundwater contribution was not simulated. An elevated nitrogen concentration during dry periods with low discharge is thought to be a result of the release of nitrogen via groundwater through-flow which experienced limited dilution before the release.

The opposite cases were observed with NO_x^--N in October and December 2012 when the NO_3^--N concentration had a skewed gamma distribution, that is, most values were very small compared to the maximum value (as shown in Figure 8b and Figures S6b and S6c in Supporting Information S1), which resulted in poor performance of the mixing model.

The Bayesian mixing model results (Figures 7a and 7b) indicate that the uncertainty due to parameters (dark gray shaded area) was less than the uncertainty due to observation (light gray area). This indicates high variance in the observation responsible for high variance in the data model probability given the model parameters at the state process $p(Y(t_i)|\psi(t_i),\theta)$, particularly NO_3^--N concentration in the dry period.

3.4. Nitrogen Export Rate

The land use-specific export rates of NO_3^--N and NH_4^+-N (mg/ha/day) presented in Table 2 were converted from the posteriors of land use specific concentration (µmol/L) (Figure 6 and Figures S4 and S5 in Supporting Information S1) using Equations 8a and 8b. During the dry period, nutrient export rates of NO_3^--N and NH_4^+-N from forest (0.01 and 0.12 mg/ha/day, respectively) and rural land uses (0.03 and 0.27 mg/ha/day, respectively) were low, urban land use produced more NO_3^--N (2.2 mg/ha/day) than any other land use, whereas wetland and livestock land uses produced more NH_4^+-N (1.3 mg/ha/day and 1.1 mg/ha/day, respectively) than the others. Nutrient export rates during the wet period were 3 orders of magnitude higher than during the dry period, with the wetland land use being the main contributor of both NO_3^--N (110 g/ha/day) and NH_4^+-N (27 g/ha/day).

The dissolved inorganic nitrogen export rates during the dry period were low (of the order of 0.1 mg/ha/day on average) compared to the rates during the wet period (NO_3^--N ranging from 0.06 g/ha/day from forest to 110 g/ha/day from wetland). The low export during dry period needs to be treated with caution. The low export rate was due to the DHM-simulated low flow, which could cause some grids lacking in wet cells exporting the nitrogen, hence low export rates.

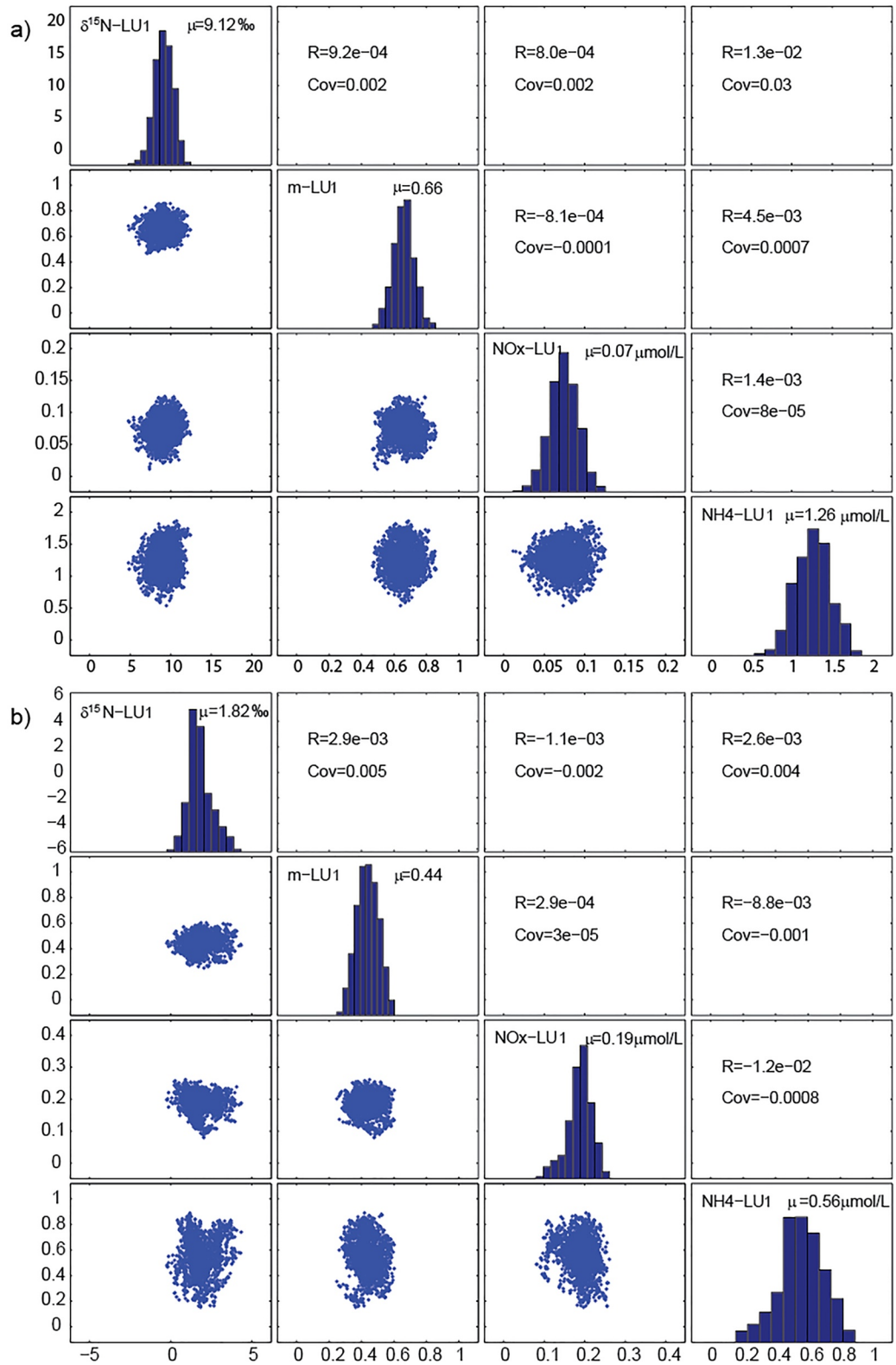

Figure 6. Parameter covariance matrix from MCMC calibration for the forest land use dry period (a) and wet period (b). Lower triangle: pairwise scatterplots of the four-parameter randomizations for forest. Upper triangle: the corresponding Pearson's correlation and Covariance coefficient. Diagonal: posterior distributions (parameters $NO_3^- N_{j,post}$ and $NH_4^+ N_{j,post}$ in Equations 7c and 7d). Plots for other land uses are provided in Supporting Information.

Table 1
Posteriors Result of Markov-Chain Monte Carlo Calibration

			Posteriors—Dry period			Posteriors—Wet period		
Land use	Parameter	Unit	μ ± σ	Min	Max	μ ± σ	Min	Max
Forest	$\delta^{15}N_{NO3}$	‰	9.1 ± 1.1	4.7	12	1.8 ± 0.84	1.1	5.0
	Gradient (m)	Dimensionless	0.66 ± 0.06	0.46	0.86	0.44 ± 0.06	0.37	0.75
	NO_3^--N	μmol/L	0.07 ± 0.02	0.01	0.12	0.19 ± 0.03	0.07	0.25
	NH_4^+-N	μmol/L	1.3 ± 0.21	0.54	1.86	0.56 ± 0.15	0.53	1.4
Rural	$\delta^{15}N_{NO3}$	‰	6.8 ± 0.83	0.77	9.1	2.2 ± 0.75	3.6	8.6
	Gradient (m)	Dimensionless	0.84 ± 0.05	0.68	0.99	0.73 ± 0.04	0.59	0.89
	NO_3^--N	μmol/L	0.20 ± 0.05	0.01	0.39	0.21 ± 0.03	0.15	0.32
	NH_4^+-N	μmol/L	1.9 ± 0.24	1.2	2.6	1.2 ± 0.19	0.61	1.8
Livestock	$\delta^{15}N_{NO3}$	‰	10 ± 1.3	6.4	14	2.2 ± 1.33	−1.9	7.6
	Gradient (m)	Dimensionless	0.87 ± 0.06	0.67	1.0	0.75 ± 0.03	0.35	0.58
	NO_3^--N	μmol/L	10 ± 0.73	7.48	12	8.7 ± 0.59	5.7	9.0
	NH_4^+-N	μmol/L	0.32 ± 0.11	0.05	0.67	0.50 ± 0.10	0.19	0.76
Crops	$\delta^{15}N_{NO3}$	‰	6.1 ± 1.15	2.6	9.50	6.6 ± 0.98	3.7	9.45
	Gradient (m)	Dimensionless	1.2 ± 0.06	0.99	1.5	0.80 ± 0.07	0.59	1.0
	NO_3^--N	μmol/L	10 ± 2.1	5.1	16	12 ± 1.8	8.0	18
	NH_4^+-N	μmol/L	0.87 ± 0.19	0.34	1.5	2.4 ± 0.23	1.7	3.0
Urban	$\delta^{15}N_{NO3}$	‰	9.2 ± 0.78	6.9	11.3	8.6 ± 0.70	8.1	12
	Gradient (m)	Dimensionless	0.70 ± 0.06	0.51	0.90	0.43 ± 0.05	0.29	0.57
	NO_x^--N	μmol/L	15 ± 2.18	8.3	22	16 ± 1.7	16	26
	NH_4^+-N	μmol/L	1.9 ± 0.27	0.99	2.7	2.6 ± 0.42	1.4	3.6
Wetland	$\delta^{15}N_{NO3}$	‰	3.2 ± 2.1	−2.0	7.0	3.4 ± 1.1	0.10	6.6
	Gradient (m)	Dimensionless	1.0 ± 0.08	0.81	1.3	0.75 ± 0.06	0.51	0.90
	NO_3^--N	μmol/L	9.2 ± 2.5	1.0	18	19 ± 2.2	11	25
	NH_4^+-N	μmol/L	8.4 ± 1.09	4.1	12	5.3 ± 0.63	3.6	7.2

4. Discussion

4.1. Nutrient Export Bayesian Model

We have presented an inverse modeling technique to estimate the land use-specific export of dissolved inorganic nitrogen (NO_3^--N and NH_4^+-N) by including isotope abundances $\delta^{15}N_{NO3}$ and $\delta^{18}O_{NO3}$, whilst simultaneously assessing uncertainty in the mixing model parameters by application of Bayesian inference within an MCMC algorithm. The model framework is flexible, that is, the probability of parameter $p(\theta)$ and the probability of state variables (model data) given the conditional posteriors $p(y|\psi,\theta)$ can be updated with more observed data which essentially reduces data variance. This in turn produces a better representation of the joint distribution for the Bayesian prediction (Figure 7). The stochastic nature inherent in the prediction and posterior inferences can be utilized to investigate the model uncertainty and variability. The first will decline with more measurements or data model $p(y)$ that reduces sample variance, but the latter will stay the same.

One problem in implementing MCMC simulations was caused by the transient phase of the Markov chain never reaching the stationary phase (Brooks & Roberts, 1998), resulting in convergence never being achieved. Cleaning-up data outliers and an investigation on the initial search and search area can reduce this problem. It is not easy to develop algorithms to achieve the convergence of the solution during a random walk Metropolis algorithm; however, the convergence process can easily be assessed using the three diagnostics (see Section 2.3.3). It should be noted that the Geweke's diagnostic attempts to verify a necessary, but not necessarily sufficient condition for convergence, as it informs us of when convergence is not achieved, but not when it does (Brooks &

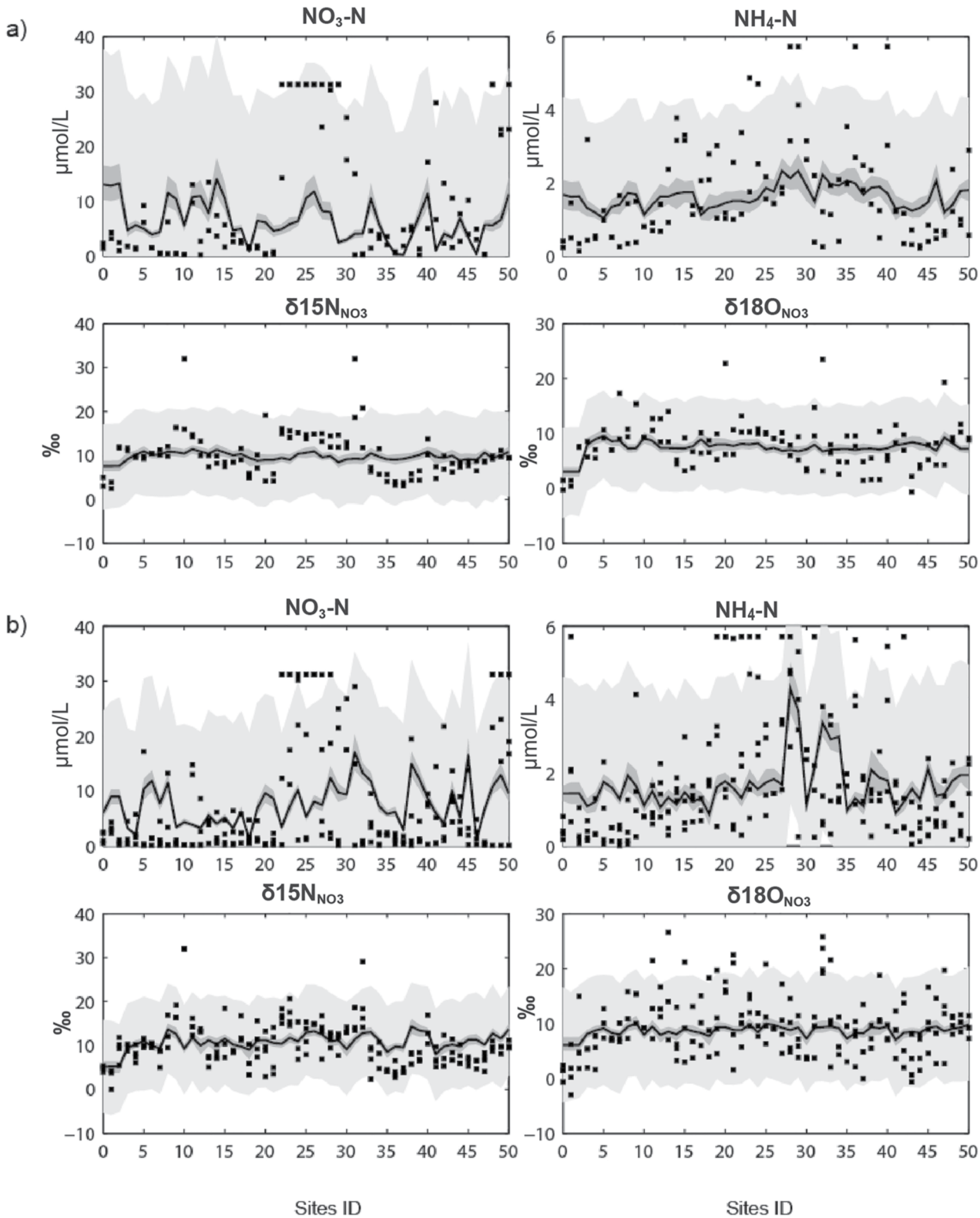

Figure 7. Observations (■) versus median values of Bayesian mixing model for all samples NO_3-N, NH_4-N, $\delta^{15}N_{NO3}$, $\delta^{18}O_{NO3}$ in: (a) the dry period and (b) the wet period. The gray zone area around the median is based on a random parameter sampling (n = 1,000) from posterior parameter distribution (MCMC calibration result), showing 95% confidence interval ($\mu \pm 1.96\delta$) for observations (light gray) and for model parameters (dark gray). Results for each wet period sampling campaign are provided in Supporting Information.

Table 2
Isotope Signature and Nitrogen Export Rates

Land use	Parameter	Unit	Isotopic signal and export rate (μ ± 1σ)		Comparison to similar system
			Dry period	Wet period	
Forest	$\delta^{15}N_{NO3}$	‰	9.1 ± 1.1	1.8 ± 0.84	Oak Ridges groundwater discharge swamp export of NO_3^--N: 9.5 kg/ha/yr (Hill, 1991).
	$\delta^{18}O_{NO3}$	‰	6.0 ± 0.96	1.3 ± 0.67	
	NO_3^--N	mg/ha/day	0.01	$(0.06 \pm 0.005) \times 10^3$	
	NH_4^+-N	mg/ha/day	0.12 ± 0.003	$(0.19 \pm 0.03) \times 10^3$	
Rural	$\delta^{15}N_{NO3}$	‰	6.8 ± 0.83	2.2 ± 0.75	
	$\delta^{18}O_{NO3}$	‰	5.7 ± 0.89	4.6 ± 0.78	
	NO_3^--N	mg/ha/day	0.03	$(0.11 \pm 0.01) \times 10^3$	
	NH_4^+-N	mg/ha/day	0.27 ± 0.004	$(0.52 \pm 0.08) \times 10^3$	
Livestock	$\delta^{15}N_{NO3}$	‰	10 ± 1.3	2.2 ± 1.3	South Pine catchment exports of NO_3^--N: 0.33 kg/ha/yr, NH_4^+-N: 0.02 kg/ha/yr (Eyre et al., 2011).
	$\delta^{18}O_{NO3}$	‰	9.2 ± 1.44	1.0 ± 0.84	
	NO_3^--N	mg/ha/day	1.1 ± 0.08	$(6.8 \pm 0.29) \times 10^3$	
	NH_4^+-N	mg/ha/day	1.1 ± 0.01	$(0.17 \pm 0.05) \times 10^3$	
Crops	$\delta^{15}N_{NO3}$	‰	6.1 ± 1.1	6.6 ± 0.98	
	$\delta^{18}O_{NO3}$	‰	7.3 ± 1.4	4.6 ± 0.72	
	NO_3^--N	mg/ha/day	1.7 ± 0.25	$(7.2 \pm 1.1) \times 10^3$	
	NH_4^+-N	mg/ha/day	0.15 ± 0.02	$(1.0 \pm 0.13) \times 10^3$	
Urban	$\delta^{15}N_{NO3}$	‰	9.2 ± 0.78	8.6 ± 0.70	North Pine catchment export of NO_3^--N: 0.29 kg/ha/yr, NH_4^+-N: 0.08 kg/ha/yr (Eyre et al., 2011).
	$\delta^{18}O_{NO3}$	‰	6.4 ± 0.80	5.2 ± 0.81	
	NO_3^--N	mg/ha/day	2.2 ± 0.34	$(16 \pm 1.7) \times 10^3$	
	NH_4^+-N	mg/ha/day	0.23 ± 0.04	$(2.3 \pm 0.37) \times 10^3$	
Wetland	$\delta^{15}N_{NO3}$	‰	3.2 ± 2.1	3.4 ± 1.1	
	$\delta^{18}O_{NO3}$	‰	3.3 ± 2.2	2.5 ± 0.87	
	NO_3^--N	mg/ha/day	1.8 ± 0.30	$(110 \pm 12) \times 10^3$	
	NH_4^+-N	mg/ha/day	1.3 ± 0.13	$(27 \pm 3.7) \times 10^3$	

Roberts, 1998). The diagnostic uses a spectral sensitivity estimate, which is also an estimator of the true variance, and brings the chains to eventually converge to the stationary distribution and the target distribution.

4.2. Role of Isotopic Abundances in Reducing Model Over-Parameterization

The effect of including $\delta^{15}N_{NO3}$ and $\delta^{18}O_{NO3}$ values in the mixing model is to add more constraints to the model parameter optimization, thereby reducing the likelihood of some parameter combinations by limiting the options of source of NO_3^- from each land use. That is without isotope data included, the cost function within the MCMC routine was applied with only two constraints NO_3-N and NH_4-N, whereas with the isotope-enabled model, there were four constraints (NO_3-N, NH_4-N, $\delta^{15}N_{NO3}$, and $\delta^{18}O_{NO3}$). This, in turn, constrains the most likely sources and pathways of nitrogen.

Comparison of the model evaluation metrics of the mixing model with (isotope-enabled) and without the inclusion of isotopes signatures (Figure 8) suggests that during the wet period the isotope-enabled model performed better, that is, less RMSE, higher correlation (r), and determination (r^2) with the observed values, and higher NSE compared to the results without isotopes application. During the dry period, differences were not significant (details in Table S3 in Supporting Information S1). The negative values of NSE for both isotope-enabled and non-isotope-enabled models for NO_3-N indicated the unacceptable performance of the export model to estimate the land use-specific nitrogen export during the dry period under assumed/available posteriors and model data. At low flow, groundwater may dominate with a non-varying N and isotope composition, and this was not simulated.

The middle panels of Figure 8 illustrate the mechanism behind the better performance of the simulation using the isotope-enabled model during the wet period. The standard deviations of the land use-specific nitrogen concentration posteriors resulting from the isotope-enabled export model were less than the deviations no-isotope model, hence less uncertainty. This resulted in the isotope-enabled export model producing values in better agreement (closer to 1:1 line) with the measured values than the no-isotope model, as shown in the top panel of Figure 8.

A sensitivity analysis was conducted to explore the effect of the concentration data distribution on model results. This was done by removing the outliers and extending the data set from 4 to 6 sampling events (Figure S8 in Supporting Information S1). The original data of CR5, C11, and CR13 were selected and bound to the 20th and 80th percentiles and, for the next three events, datasets were modified by increasing the concentrations by 3% and reducing the flows by 3%. Isotope abundances were unaltered. The results shown in the lower panels of Figure 8 indicate an improvement in the metrics of determination (r^2), NSE, and RSR for NO_3-N, suggesting the data distribution does influence the model results.

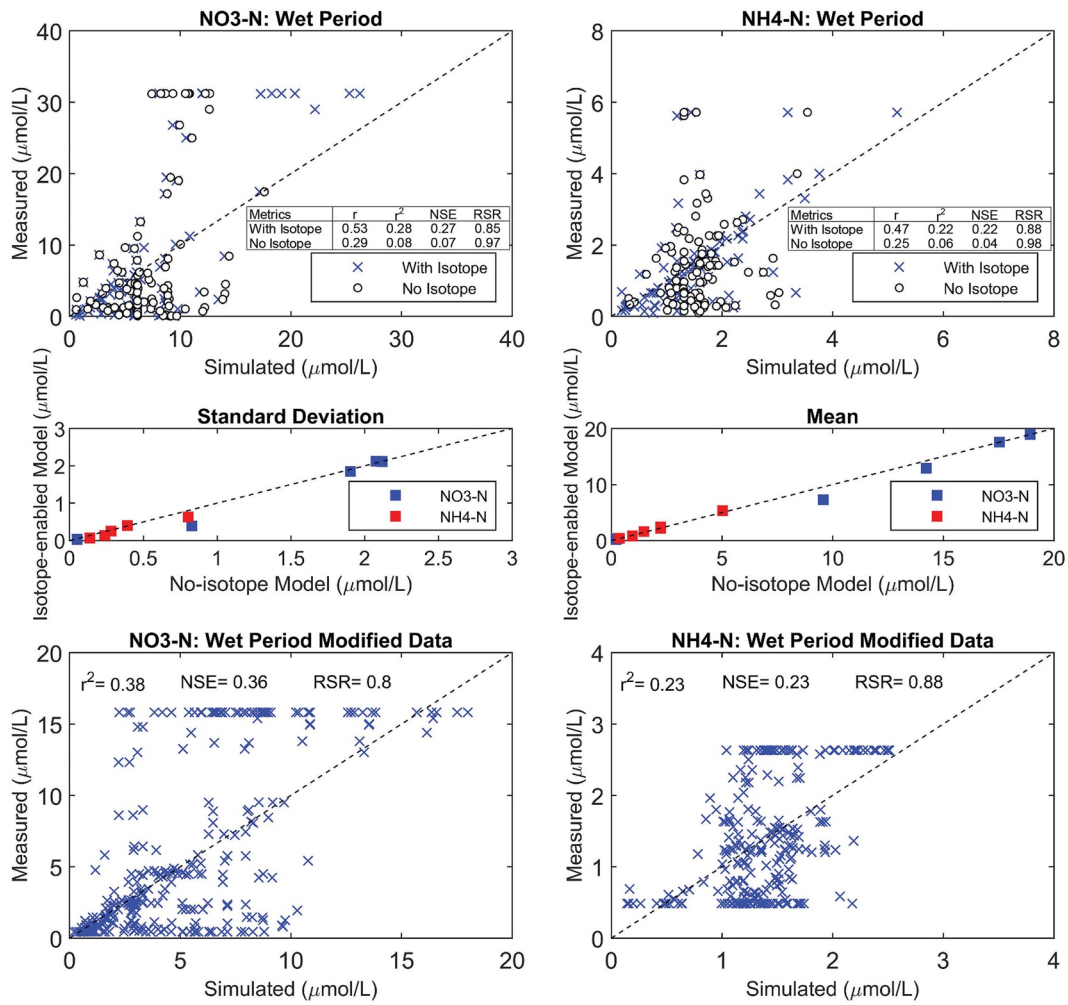

Figure 8. Comparison of isotope-enabled and no-isotope export model of NO_3-N and NH_4-N concentrations versus observations in wet period plotted in 1:1 line (top panels), mean and standard deviation of the posteriors (middle panels) and results from modified data (bottom panels).

4.3. Isotope Signature

The comparison of isotope signatures between land use during dry and wet periods (Table 1) indicates that $\delta^{15}N_{NO3}$ signatures of forest, rural, and livestock in the dry period were significantly higher than in the wet period. The isotope shifts (i.e., enrichment in ^{15}N) between dry and wet periods could be also caused by denitrification as a function of the fraction of residual NO_x-N (Rassam et al., 2008).

Signatures of urban $\delta^{15}N_{NO3}$ for both the dry and wet periods (ranging from +6.9‰ to +12‰) are generally higher than the other land uses. This may be due to typical $\delta^{15}N_{NO3}$ signatures in stormwater and sewage ranging from +7‰ to +20‰, compared to signatures in atmospheric deposition $\delta^{15}N_{NO3}$ from −10‰ to +8‰ (Kendall et al., 2007), $\delta^{15}N_{NO3}$ vehicle emissions +3.7‰, and roadside vegetation +3.8‰ (Elliott et al., 2007).

Signatures of $\delta^{18}O_{NO3}$ can be used to inform the proportion of oxygen sources which can be from precipitation ($\delta^{18}O_{H2O}$ −4‰ to −3‰; Hollins et al., 2018), H_2O in soil zone ($\delta^{18}O_{H2O}$ −30‰ to 5‰; Kendall, 1998), microbial respiration O_2 (high $\delta^{18}O_{O2}$ as a result of isotopic fractionation) or atmospheric O_2 ($\delta^{18}O_{O2}$ +23‰; Kroopnick & Craig, 1972). The comparisons of $\delta^{18}O_{NO3}$ between the dry and the wet periods for each land use (Table 2) show consistently that the signatures are higher in the dry period than in the wet period, which indicates that the main source of oxygen is microbial respiration.

Figure 9 illustrates that Lagoon-King John Creek experienced more biogeochemical transformation compared to other streams, suggesting the release of dissolved inorganic nitrogen in a mixing environment (indicated by a similar rate of change of $\delta^{15}N_{NO3}$ and $\delta^{18}O_{NO3}$) from upstream (station 19) to station 28, then denitrification around stations 34–35 (located next to landfill) (Figure 9b), followed with mineralization and nitrification, and possibly N-fixation downstream in area dominated by forest land use (Figures 9a–9d).

Isotope signatures during dry periods may be a good representation of a typical signature of soil. Table 2 shows that in the dry periods, signals of $\delta^{15}N_{NO3}$ in forests and livestock are higher than in crops and rural. This may be due to uncultivated soils having slightly higher $\delta^{15}N_{NO3}$ signal natural soils (−3‰ to +5‰) or N produced by nitrification in green manure soil (−20‰ to +10‰) compared to cultivated soils which use anthropogenic NO_3^--N and NH_4^+-N such as synthetic fertilizer ($\delta^{15}N \approx 0$‰) (Kendall et al., 2007).

The gradient (m) values of $0.5 < m < 1$ in the $\delta^{18}O_{NO3}$ and $\delta^{15}N_{NO3}$ linear regression (Table 1), or between 1:1 (mixing line) and 2:1 denitrification line of Kendall et al. (2007), suggest that generally NO_3^--N experienced mixing and denitrification in the soil and riparian zones once it was exported off the land use, except for crops and wetland land uses in the dry periods where their gradients tend toward the nitrification line ($m > 1$).

4.4. Source of Uncertainty in Land Use-Specific Nutrient Export Rate

The accuracy of the proposed framework depends significantly upon the accuracy of the identification of land use type, and this was surveyed to validate an existing land use map provided by the Moreton Bay Regional Council (MBRC).

The DHM-modeled discharges for the dry period were small and showed insignificant differences between land use. This was reflected as uncertainty in the model due to parameter $p(\psi|\theta)$ which resulted in poor performance of the model at low flow as shown in Figure 7. Bias in the flow estimate contributed little to the model uncertainty for the wet period as the mixing model calculates the proportion of flow rather than the total flow to produce the contribution of each land use to the nutrient concentrations (Equations 7a–7e).

The higher uncertainty due to observation compared to that due to model parameters (Figure 7 and Figure S6 in Supporting Information S1) indicates that the probability of model parameters conditional on the data model $p(\psi, \theta|y)$ is more significant than the probability of model parameters given the process model or posteriors $p(\theta|\psi)$. The uncertainty represents heterogeneity in hydrogeochemical processes during the sampling events and heterogeneity in nitrogen initial distribution as legacy source of nitrogen. Such uncertainty could be reduced with more observations that reflect the spatial and temporal variation of the nitrogen export, with the capability to quantify the proportion of active and legacy source of nitrogen, which is important in managing effective water quality improvement of downstream environment (Basu et al., 2022; Chen et al., 2021).

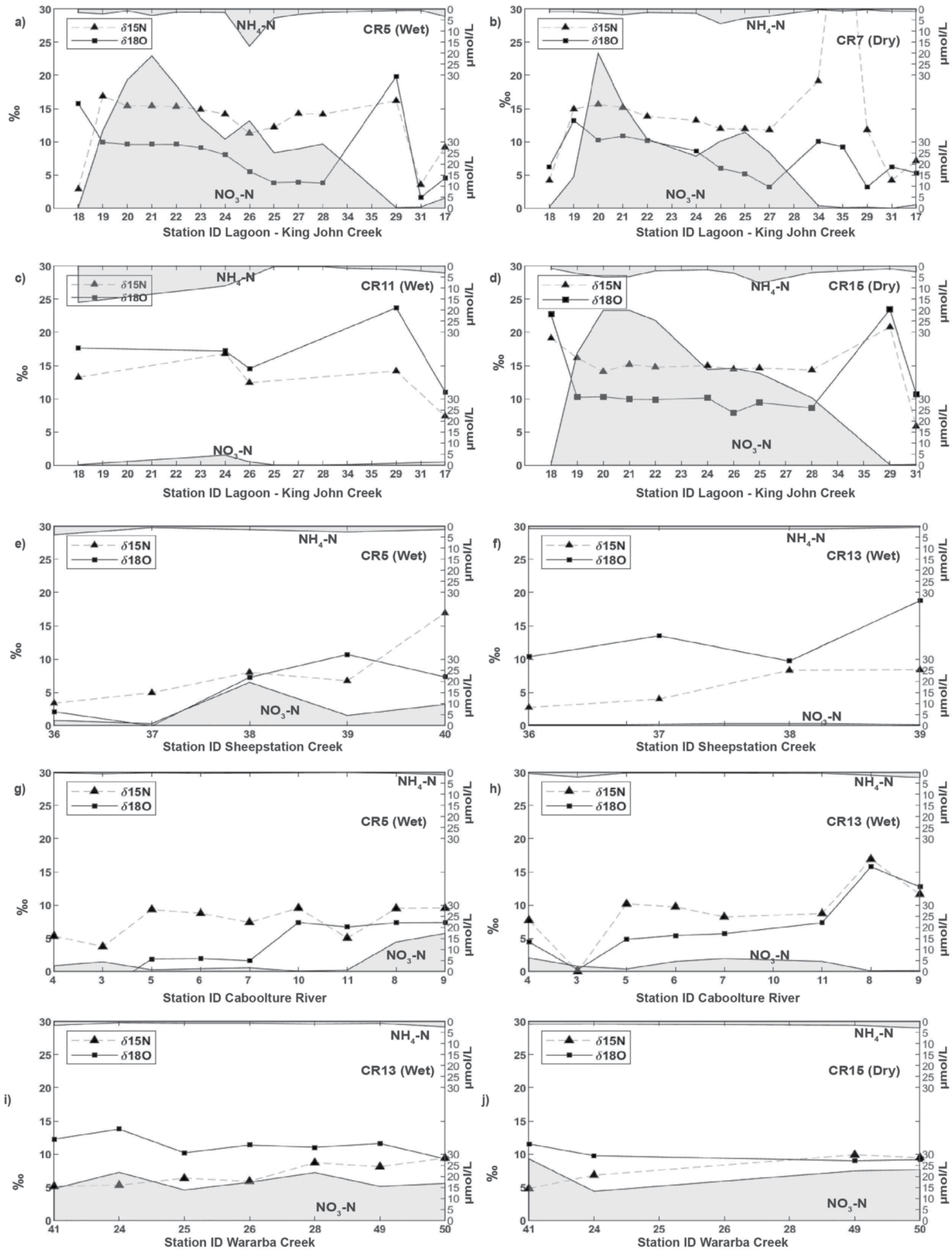

Figure 9. Example of multiple axis plots of dual isotopes $\delta^{18}O_{NO3}$–$\delta^{15}N_{NO3}$ (left *Y*-axis) and NO_3-N and NH_4-N concentrations (right *Y*-axis) along King-John Creek, Sheepstation Creek, Caboolture River, and Wararba Creek. Refer to Figure 1 for sampling station locations.

In addition, this study only included dissolved inorganic nitrogen. Approximately 3%–25% of the total nitrogen in Caboolture River catchment is exported as particulate nitrogen. Including particulate nitrogen concentration and $\delta^{15}N$ of particulate nitrogen may also improve the accuracy of the proposed framework.

5. Conclusions

This paper presents an approach that inversely estimates the land use-specific nutrient export rate using Bayesian Framework MCMC. The approach is able to provide the uncertainty estimates of the dual isotopes $\delta^{15}N_{NO3}$ and $\delta^{18}O_{NO3}$ and the concentration of dissolved nitrogen NO_3^--N and NH_4^+-N released from forest, rural, livestock, crops, urban, and wetland for wet period. During the dry period, the export rates of NO_3^--N and NH_4^+-N from forest and rural land uses were insignificant; urban land use produced more NO_3^--N than any other land uses, whereas wetland and livestock land uses produced more NH_4^+-N than the others. The export rates of dissolved inorganic nitrogen during the wet period were 3 orders of magnitude higher than during the dry period, with the main source found to be wetland (110 g/ha/day NO_3^--N and 27 g/ha/day NH_4^+-N) resulted from mineralization and nitrification of organic N, followed by urban (16 g/ha/day NO_3^--N and 2.3 g/ha/day NH_4^+-N).

The poorer Bayesian model application for the dry period (as shown with negative NSE) where elevated nutrient concentrations are released during low flow conditions suggests that the a priori mixing assumption is not valid. Thus, the approach fails. During this condition, export pathways are reduced, and soil and biogeochemical processes dominate (which were not modeled); hence, isotopic fractionation is more pronounced than isotopic mixing. This is consistent with the gradient (m) values of $0.5 < m < 1$ in the $\delta^{18}O_{NO3} = f(\delta^{15}N_{NO3})$ relationship, which suggests that generally NO_3^--N experiences mixing and denitrification once it is exported off the land use.

Conflict of Interest

The authors declare no conflicts of interest relevant to this study.

Data Availability Statement

The executable files of the hydrological model and data set for the calibration and validation used to create Figure 5 can be found at: http://doi.org/10.5281/zenodo.6812670. Original MCMC toolbox for Matlab is available on-line from: https://mjlaine.github.io/mcmcstat/.

Acknowledgments
The authors are indebted to Jessica Mowat of Moreton Bay Regional Council (MBRC), who provided valuable support and assistance with necessary data. Financial support was provided primarily by the Australian Research Council (Grant LP110200975). Financial support to visiting researcher Yasuyuki Maruya was provided by JSPS KAKENHI (JP14J03382 and JP21H05178). The authors also thank the editors and the two anonymous reviewers for their thorough reviews, insightful comments, and suggestions. Open access publishing facilitated by The University of Western Australia, as part of the Wiley - The University of Western Australia agreement via the Council of Australian University Librarians.

References

Adiyanti, S., Eyre, B. D., Maher, D. T., Santos, I., Golsby-Smith, L., Mangion, P., & Hipsey, M. R. (2016). Stable isotopes reduce parameter uncertainty of an estuarine carbon cycling model. *Environmental Modelling & Software*, *79*, 233–255. https://doi.org/10.1016/j.envsoft.2016.02.011

Arhonditsis, G. B., Perhar, G., Zhang, W., Massos, E., Shi, M., & Das, A. (2008). Addressing equifinality and uncertainty in eutrophiction models. *Water Resources Research*, *44*, W01420. https://doi.org/10.1029/2007WR005862

Basu, N. B., Destouni, G., Jawitz, J. W., Thompson, S. E., Loukinova, N. V., Darracq, A., et al. (2010). Nutrient loads exported from managed catchments reveal emergent biogeochemical stationarity. *Geophysical Research Letters*, *37*, L23404. https://doi.org/10.1029/2010GL045168

Basu, N. B., Van Meter, K. J., Byrnes, D. K., Van Cappellen, P., Brouwer, R., Jacobsen, B. H., et al. (2022). Managing nitrogen legacies to accelerate water quality improvement. *Nature Geosicence*, *15*, 97–105. Retrieved from https://www.nature.com/articles/s41561-021-00889-9

Bennett, N. D., Croke, B. F., Guariso, G., Guillaume, J. H., Hamilton, S. H., Jakeman, A. J., et al. (2013). Characterising performance of environmental models. *Environmental Modelling & Software*, *40*, 1–20. https://doi.org/10.1016/j.envsoft.2012.09.011

Böhlke, J. K., & Coplen, T. B. (1995). Interlaboratory comparison of reference materials for nitrogen isotope ratio measurements. Paper presented at Reference and Intercomparison Materials For Stable Isotopes of Light Elements, 1–3 December 1993. International Atomic Energy Agency.

Böhlke, J. K., Mroczkowski, S. J., & Coplen, T. B. (2003). Oxygen isotopes in nitrate: New reference materials for $^{18}O:^{17}O:^{16}O$ measurements and observations on nitrate-water equilibration. *Rapid Communications in Mass Spectrometry*, *17*, 1835–1846. https://doi.org/10.1002/rcm.1123

Brooks, S. P., & Roberts, G. O. (1998). Convergence assessment techniques for Markov chain Monte Carlo. *Statistics and Computing*, *8*, 319–335. https://doi.org/10.1023/A:1008820505350

Casciotti, K. L., Sigman, D. M., Hastings, M. G., Bohlke, J. K., & Hilkert, A. (2002). Measurement of the oxygen isotopic composition of nitrate in seawater and freshwater using the denitrifier method. *Analytical Chemistry*, *74*, 4905–4912. https://doi.org/10.1021/ac020113w

Chen, Y., Destouni, G., Goldenberg, R., & Prieto, C. (2021). Nutrient source attribution: Quantitative typology distinction of active and legacy source contributions to waterborne loads. *Hydrological Processes*, *35*, 14284. https://doi.org/10.1002/hyp.14284

Duan, Q. Y., Gupta, V. K., & Sorooshian, S. (1993). Shuffled complex evaluation approach for effective and efficient global minimisation. *Journal of Optimization Theory and Applications*, *76*(3), 501–521. https://doi.org/10.1007/bf00939380

Duan, Q. Y., Sorooshian, S., & Gupta, V. K. (1994). Optimal use of the SCE-UA global optimisation method for calibrating watershed models. *Journal of Hydrology*, *158*, 265–284. https://doi.org/10.1016/0022-1694(94)90057-4

Elliott, E. M., Kendall, C., Wankel, S. D., Burns, D. A., Boyer, E. W., Harlin, K., et al. (2007). Nitrogen isotopes as indicators of NO_x source contributions to atmospheric nitrate deposition across the Midwestern and Northeastern United States. *Environmental Science & Technology*, *41*(22), 7661–7667. https://doi.org/10.1021/es070898t

Erler, D. V., Duncan, T. M., Murray, R., Maher, D. T., Santos, I. R., Gatland, J. R., et al. (2015). Applying cavity ring-down spectroscopy for the measurement of dissolved nitrous oxide concentrations and bulk nitrogen isotopic composition in aquatic systems: Correcting for interferences and field application. *Limnology and Oceanography: Methods*, *13*, 391–401. https://doi.org/10.1002/lom3.10032

Eyre, B. D. (2000). Regional evaluation of nutrient transformation and phytoplankton growth in nine river-dominated sub-tropical east Australian estuaries. *Marine Ecology Progress Series*, *205*, 61–83. https://doi.org/10.3354/meps205061

Eyre, B. D., Ferguson, A. J. P., Webb, A., Maher, D., & Oakes, J. M. (2011). Denitrification, N-fixation and nitrogen and phosphorus fluxes in different benthic habitats and their contribution to the nitrogen and phosphorus budgets of a shallow oligotrophic sub-tropical coastal system (southern Moreton Bay, Australia). *Biogeochemistry*, *102*, 111–133. https://doi.org/10.1007/s10533-010-9425-6

Eyre, B. D., Maher, D. T., & Sanders, C. (2016). The contribution of denitrification and burial to the nitrogen budgets of three geomorphically distinct Australian estuaries: Importance of seagrass habitats. *Limnology & Oceanography*, *61*(3), 1144–1156. https://doi.org/10.1002/lno.10280

Eyre, B. D., & Pont, D. (2003). Intra- and inter-annual variability in the different forms of diffuse nitrogen and phosphorus delivered to seven sub-tropical east Australian estuaries. *Estuarine, Coastal and Shelf Science*, *57*, 137–148. https://doi.org/10.1016/S0272-7714(02)00337-2

Ford, W. I., Fox, J. F., & Pollock, E. (2017). Reducing equifinality using isotopes in a process-based stream nitrogen model highlights the flux of algal nitrogen from agricultural streams. *Water Resources Research*, *53*, 6539–6561. https://doi.org/10.1002/2017WR020607

Gall, H. E., Park, J., Harman, C. J., Jawitz, J. W., & Rao, P. S. C. (2013). Landscape filtering of hydrologic and biogeochemical responses in managed catchments. *Landscape Ecology*, *28*(4), 651–664. https://doi.org/10.1007/s10980-012-9829-x

Geweke, J. (1992). Evaluating the accuracy of sampling based approaches to the calculation of posterior moments. In J. M. Bernardo, J. Berger, & A. P. Dawid (Eds.), *Bayesian statistics* (pp. 169–193).

Grabe, M. (2010). *Generalized Gaussian error Calculus* (p. 301). Springer-Verlag.

Gunaratne, G. L., Vogwill, R. I. J., & Hipsey, M. R. (2017). Effect of seasonal flushing on nutrient export characteristics of an urbanizing, remote, ungauged coastal catchment. *Hydrological Sciences Journal*, *62*(5), 800–817. https://doi.org/10.1080/02626667.2016.1264585

Haario, H., Laine, M., Mira, A., & Saksman, E. (2006). DRAM: Efficient adaptive MCMC. *Statistics and Computing*, *16*, 339–354. https://doi.org/10.1007/s11222-006-9438-0

Harmon, R., & Challenor, P. (1997). A Markov chain Monte Carlo method for estimation and assimilation into models. *Ecological Modelling*, *101*(1), 41–59. https://doi.org/10.1016/s0304-3800(97)01947-9

Hill, A. R. (1991). A groundwater nitrogen budget for a headwater swamp in an area of permanent groundwater discharge. *Biogeochemistry*, *14*, 209–224. https://doi.org/10.1007/bf00000808

Hollins, S. E., Hughes, C. E., Crawford, J., Cendon, D. I., & Meredith, K. T. (2018). Rainfall isotope variations over the Australian continent – Implications for hydrology and isoscape applications. *Science of the Total Environment*, *645*, 630–645. https://doi.org/10.1016/j.scitotenv.2018.07.082

Houska, T., Kraft, P., Liebermann, R., Klatt, S., Krauss, D., Haas, E., et al. (2017). Rejecting hydro-biogeochemical model structures by multi-criteria evaluation. *Environmental Modelling & Software*, *93*, 1–12. https://doi.org/10.1016/j.envsoft.2017.03.005

Hunukumbura, P. B., Tachikawa, Y., & Shiiba, M. (2012). Distributed hydrological model transferability across basins with different physico-climatic characteristics. *Hydrological Processes*, *26*(6), 793–808. https://doi.org/10.1002/hyp.8294

Kang, X., Niu, Y., Yu, H., Gou, P., Hou, Q., Lu, X., & Wu, Y. (2022). Effect of rainfall-runoff process on sources and transformations of nitrate using a combined approach of dual isotopes, hydrochemical and Bayesian model in the Dagang River basin. *Science of The Total Environment*, *837*, 155674. https://doi.org/10.1016/j.scitotenv.2022.155674

Kendall, C. (1998). Tracing nitrogen sources and cycling in catchments. In C. Kendall, & J. J. McDonnell (Eds.), *Resources on isotopes* (pp. 519–576). Elsevier Science B.V. https://doi.org/10.1016/b978-0-444-81546-0.50023-9

Kendall, C., Elliott, E. M., & Wankel, S. D. (2007). Tracing anthropogenic inputs of nitrogen to ecosystems. In R. Michener, & K. Lajtha (Eds.), *Stable isotopes in eology and environmental science*. Blackwell Publishing.

Kroopnick, P., & Craig, H. (1972). Atmospheric oxygen: Isotopic composition and solubility fractionation. *Science*, *175*, 54–55. https://doi.org/10.1126/science.175.4017.54

Lee, K. S., Bong, Y. S., Lee, D., Kim, Y., & Kin, K. (2008). Tracing the source of nitrate in the Han River watershed in Korea, using $\delta^{15}N-NO_3-$ and $\delta^{18}O-NO_3-$ values. *Science of the Total Environment*, *395*, 117–124. https://doi.org/10.1016/j.scitotenv.2008.01.058

Liu, X.-L., Han, G., Zeng, J., Liu, M., Li, X.-Q., & Boeckxc, P. (2021). Identifying the sources of nitrate contamination using a combined dual isotope, chemical and Bayesian model approach in a tropical agricultural river: Case study in the Mun River, Thailand. *Science of The Total Environment*, *760*, 143938. https://doi.org/10.1016/j.scitotenv.2020.143938

Mayer, B., Boyer, E. W., Goodale, C., Jaworski, N. A., VanBreemen, N., Howarth, R. W., et al. (2002). Sources of nitrate in rivers draining sixteen watersheds in the northeastern U.S: Isotopic constraints. *Biogeochemistry*, *57/58*, 171–197. https://doi.org/10.1023/A:1015744002496

McKee, L., Eyre, B. D., & Hossain, S. (2000). Intra- and inter-annual export of nitrogen and phosphorus in the sub-tropical Richmond River catchment, Australia. *Hydrological Processes*, *14*, 1787–1809. https://doi.org/10.1002/1099-1085(200007)14:10<1787::AID-HYP42>3.0.CO;2-Z

Moriasi, D. N., Arnold, J. G., Liew, M. W. V., Bingner, R. L., Harmel, R. D., & Veith, T. L. (2007). Model evaluation guidelines for systematic quantification of accuracy in watershed simulations. *American Society of Agricultural and Biological Engineers*, *50*(3), 885–900.

Nash, J. E., & Sutcliffe, V. (1970). River flow forecasting through conceptual models. Part 1 – A discussion of principles. *Journal of Hydrology*, *10*, 282–290. https://doi.org/10.1016/0022-1694(70)90255-6

Oldham, C. E., Farrow, D. E., & Peiffer, S. (2013). A generalized Damköhler number for classifying material processing in hydrological systems. *Hydrology and Earth System Sciences*, *17*, 1133–1148. https://doi.org/10.5194/hess-17-1133-2013

Paniconi, C., & Putti, M. (2015). Physically based modeling in catchment hydrology at 50: Survey and outlook. *Water Resources Research*, *51*, 7090–7129. https://doi.org/10.1002/2015WR017780

Peters, N. E., Böhlke, J. K., Brooks, P. D., Burt, T. P., Gooseff, M. N., Hamilton, D. P., et al. (2011). Hydrology and biogeochemistry linkages. In P. Wilderer (Ed.), *Treatise on water science* (Vol. 2, pp. 271–304). Academic Press. https://doi.org/10.1016/b978-0-444-53199-5.00038-5

Phillips, D. L., Newsome, S. D., & Gregg, J. W. (2005). Combining sources in stable isotope mixing models: Alternative methods. *Oecologia*, *144*, 520–527. https://doi.org/10.1007/s00442-004-1816-8

Rassam, D. W., Pagendam, D. E., & Hunter, H. M. (2008). Conceptualisation and application of models for groundwater–surface water interactions and nitrate attenuation potential in riparian zones. *Environmental Modelling & Software*, *23*(7), 859–875. https://doi.org/10.1016/j.envsoft.2007.11.003

Saeck, E. A., O'Brien, K. R., Weber, T. R., & Burford, M. A. (2013). Changes to chronic nitrogen loading from sewage discharges modify standing stocks of coastal phytoplankton. *Marine Pollution Bulletin*, *71*, 159–167. https://doi.org/10.1016/j.marpolbul.2013.03.020

Sayama, T., & McDonnell, J. J. (2009). A new time-space accounting scheme to predict stream water residence time and hydrograph source components at the watershed scale. *Water Resources Research*, *45*, W07401. https://doi.org/10.1029/2008WR007549

Seitzinger, S. P., Mayorga, E., Bouwman, A. F., Kroeze, C., Beusen, A. H. W., Billen, G., et al. (2010). Global river nutrient export: A scenario analysis of past and future trends. *Global Biogeochemical Cycles*, *24*, GB0A08. https://doi.org/10.1029/2009GB003587

Sigman, D. M., Casciotti, K. L., Andreani, M., Barford, C., Galanter, M., & Bohlke, J. K. (2001). A bacterial method for the nitrogen isotopic analysis of nitrate in seawater and freshwater. *Analytical Chemistry*, *73*, 4145–4153. https://doi.org/10.1021/ac010088e

Smith, V. H. (2006). Responses of estuarine and coastal marine phytoplankton to nitrogen and phosphorus enrichment. *Limnology & Oceanography*, *51*(1), 377–384. https://doi.org/10.4319/lo.2006.51.1_part_2.0377

Tanaka, T., & Tachikawa, Y. (2015). Testing the applicability of a kinematic wave-based distributed hydrologic model in two climatically contrasting catchments. *Hydrological Sciences Journal*, *60*(7–8), 1361–1373. https://doi.org/10.1080/02626667.2014.967693

Tanaka, T., Thiha, S., Tachikawa, Y., & Yorozu, K. (2015). Improvement of a kinemative wave-based distributed hydrologic model to predict flow regimes in arid areas. Climate change and water & environment management in monsoon Asia.

Turner, J. V., Albrechtsen, H.-J., Bonell, M., Duguet, J.-P., Harris, B., Meckenstock, R., et al. (2006). Future trends in transport and fate of diffuse contaminants in catchments with special emphasis on stable isotope applications. Scientific Briefing of a UNESCO Integrated Science Initiative Workshop GSF, Neuherberg, Germany, 30 November to 2 December 2004. *Hydrological Processes*, *20*, 205–213. https://doi.org/10.1002/hyp.6074

Voss, M., Deutsch, B., Elmgren, R., Humborg, C., Kuuppo, P., Pastuszak, M., et al. (2006). Source identification of nitrate by means of isotropic tracers in the Baltic Sea catchments. *Biogeosciences*, *3*, 663–676. https://doi.org/10.5194/bg-3-663-2006

Zhang, W., & Arhonditsis, G. B. (2009). A Bayesian hierarchical framework for calibrating aquatic biogeochemical models. *Ecological Modelling*, *220*, 2142–2161. https://doi.org/10.1016/j.ecolmodel.2009.05.023